UNIVERSITY OF CALIFORNIA, SAN DIEGO

Surround Processing in the Awake Rodent dLGN

A dissertation submitted in partial satisfaction of the
requirements for the degree
Doctor of Philosophy

in

Biology

by

Balaji Sriram

Committee in charge:

Professor Pamela Reinagel, Chair
Professor Edward Callaway
Professor Timothy Gentner
Professor Stefan Leutgeb
Professor Massimo Scanziani

2012

The dissertation of Balaji Sriram is approved, and it is acceptable in quality and form for publication on microfilm and electronically:

_____

_____

_____

_____

_____
Chair

University of California, San Diego

2012

DEDICATION

To my parents, for teaching me how to dream.

TABLE OF CONTENTS

LIST OF FIGURES

ACKNOWLEDGEMENTS

My doctoral work has been the result of many collaborations, explicit and implicit. To start with, I would like to thank my principal collaborator and my boss for the last four years, Pamela Reinagel. This document owes a lot to the constant support and direction provided by her. I am especially grateful for the relentless focus towards the big picture that she has provided. If I get to retain one thing from my last four years, that would be it.

Another formative aspect of my graduate studies is the excellent intellectual environment provided within my lab. I was lucky to have the company of three amazing graduate students: Philip Meier, Erik Flister and Claire Discenza. To Phil and Erik: thanks for making my transition from engineer to neuroscientist easy. Late night recording sessions would have been unbearable without your company. To Claire: thank you for teaching me anatomy and for being a supportive labmate through happy times and hard times. One other person whose presence heavily influenced my PhD experience is Sarah, lab manager extraordinaire. Your support and asssistance was critical to my graduate experience

This acknowledgements section will be grossly inadequate without the mention of my friends. I'd like to thank Jeff Moore and Aleena Garner Wednesday nights. I hope we get to have a few more of those nights sometime. Harish Nagarajan and Arun Manohar were great anchors throughout my grad life and were critical in helping me establish a sense of balance to my life.

Finally, I would like to thank my family. Madhubala, my sister, for being a wonderful teacher and student. And my parents: you are an inspiration to me. Thanks for standing by my career choice. Thanks for your encouragement no matter what the circumstance. And thanks for being the coolest people I know.

Chapter 2, in part, has been submitted for publication of material as it may appear in Journal of Vision, 2012. The dissertation author is the primary investigator and the first author of the paper.

Chapter 3, in part, is being prepared for submission for publication of material. Sriram, Balaji; Reinagel, Pamela. The dissertation author was the primary investigator and the first author of the paper.

Chapter 4, in part, is being prepared for submission for publication of material. Sriram, Balaji; Reinagel, Pamela. The dissertation author was the primary investigator and the first author of the paper.

VITA

2006	B.Tech. in Biotechnology, Indian Institute of Technology, Madras
2007-2012	Graduate Teaching Assistant, University of California, San Diego
2012	Ph. D. in Biology, University of California, San Diego

PUBLICATIONS

Balaji Sriram and Pamela Reinagel, "Strong surround in the Awake Rodent dLGN", *Journal of Vision*, 314, 2012.

ABSTRACT OF THE DISSERTATION

Surround Processing in the Awake Rodent dLGN

by

Balaji Sriram

Doctor of Philosophy in Biology

University of California, San Diego, 2012

Professor Pamela Reinagel, Chair

The early visual system is responsible for encoding a complex spatiotemporal pattern of light. It transform this pattern into spikes which can then be read by downstream neurons. What strategies should neurons employ while transforming the input pattern? In the best of all possible worlds, neurons encode only information that other nearby neurons havent already encoded leading to a highly sparse highly non-redundant coding scheme. What receptive field features lead to such a sparse, non-redundant coding scheme. For linear receptive fields, the presence of a classical surround correlates well with the response sparseness and de-correlatation. I measure the strength of this surround in the rodent dLGN and find that the surround strength in the un-anesthetized rodent is optimized for maximal sparseness and decorrelation for a majority of cells. Apart from the linear

receptive field, neurons in the dLGN of many species are known to have powerful non-linear processing. Further, multiple response features of dLGN neurons have been attributed to these non-linear effects. I show that a simple linear model is capable of explaining many of these features. However, I identify multiple other response features that linear models are inherently incapable of explaining. I show that rodent dLGN neurons show atleast some of these features.

Chapter 1

Introduction

The early visual system is designed to transform complex spatio-temporal patterns of light into neuronal spikes which can then be decoded by downstream neurons. What is the essence of this transformation? i.e. What should each neuron respond to? Under constraints of efficiency, each spike a neuron sends should be as informative as possible and care should be taken to remove redundancy in the information sent. In this chapter, I discuss this primal function of the early visual system and identify some strategies it uses to achieve this function. In particular, I concentrate on the function of the dorsal Lateral Geniculate Nucleus, the primary retino-recepient nucleus. I then introduce the content of my thesis.

The dorsal Lateral Geniculate Nucleus receives its primary input from the Retinal Ganglion Cells (RGCs) in the retina and sends its primary output to Layer 4 neurons in the Primary Visual Cortex (V1). Historically dLGN neurons were among the first to be recorded and over the past fifty years the responses of these neurons have been recorded and cataloged in a variety of species and to a variety of stimuli. Due to the substantial similarities between retinal and dLGN responses it was long thought that primary function of the dLGN is to relay, essentially unchanged, retinal outputs to V1. However, recent evidence indicate that the dLGN plays a more dynamic role in encoding stimuli both under normal conditions as well as under altered mental states (sleep, inattentiveness, etc.).

What do the receptive fields of dLGN neurons look like? Much like its retinal inputs, dLGN cells have circular-concentric center-surround receptive fields

[Kuffler, 1953, Hubel and Wiesel, 1961, Rodieck and Stone, 1965, Rodieck, 1965]. Recent theoretical work suggests that the presence of antagonistic surrounds may be optimal for encoding naturalistic stimuli [Karklin and Simoncelli, 2011]. What, then should the strength of these surrounds be? Theoretical work [Atick and Redlich, 1992, Graham et al., 2006] has provided a clear understanding of the role that surrounds play in encoding naturalistic stimuli and experimental evidence has borne some of these predictions [Muller and Dacheux, 1997]. However, it is still unclear whether surrounds are important in the awake animal. The ability to measure these surrounds in the awake preparation is a critical step towards future experiments aimed at modulating their strength, pehaps by manipulating specific neuronal subtypes.

In this thesis

In my thesis, I ask the most basic questions about the structure of surrounds in the awake rodent dLGN.

In chapter 2, I discuss the importance of the classical, linear center surround architecture of dLGN neurons. This chapter aims to measure the classical surround size and strength. In it, I show that the strength of the surround is strong compared to the strength of the center in the awake rodent dLGN. Such responses enable sparse and decorrelated output from the dLGN allowing for a high SNR input into the next level of visual processing, V1.

In chapter 3, I introduce the concept of the non-classical receptive field and discuss how these are modeled. I challenge these models with well known feature of real dLGN neurons and discuss the strengths and weaknesses of each model

Finally in chapter 4, I provide size-tuning measurements obtained in the awake rodent dLGN. Many of the responses do not fit prior expectations about the kind of responess that are possible.

Chapter 2

Strong Surround Antagonism

Classical center-surround antagonism in the early visual system is thought to serve important functions such as enhancing edge detection and increasing sparseness. The relative strength of the center and surround determine the specific computation achieved; balanced surrounds are useful for decorrelating responses, while weak surrounds are better for denoising. Surround strength has been measured in the retina and dorsal Lateral Geniculate Nucleus (dLGN), primarily in anesthetized or ex vivo preparations. Here we revisit the center-surround architecture of dLGN neurons in the unanesthetized rat. We report the spatial frequency tuning of N=47 neurons. We fit these tuning curves to a difference-of-Gaussians (DOG) model of the spatial receptive field. We find that some dLGN neurons in the unanesthetized rat (N=8/47) have weak surrounds. The majority of cells in our sample (N=29/47), however, have well-balanced center and surround strengths and band-pass tuning curves. We also observed several neurons (N=10/47) with notched or dual-band-pass tuning curves, which could be explained by DOG models with extra-strong surrounds. It remains to be determined what advantage if any is conferred by the heterogeneity of surround strength. We conclude that surround antagonism can be strong in the dLGN of the unanesthetized rat.

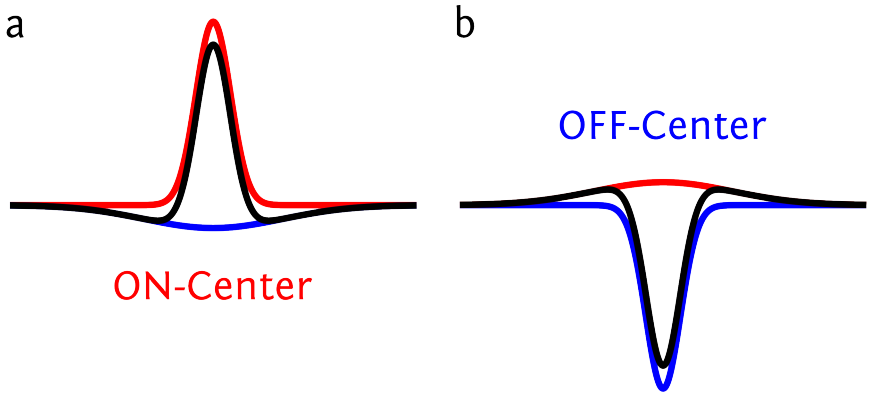

Figure 2.1: **Sensitivity profile of dLGN ON- and OFF- center cells**. The red curve in both figures refer to the ON-component and responds to an *increase* in luminance at a specific spot by increasing firing rate proportional to the value of the sensitivity at that spot. Analagously, the blue curve in each figure is the OFF-component. This component responds to a *reduction* in luminance by a proportional increase in the response.

2.1 Introduction

One of the most striking and consistent feature of early stages of sensory processing is the presence of center-surround antagonism. First described in the retina [Kuffler, 1953] and dLGN [Hubel and Wiesel, 1961], this manifests as neurons having concentric receptive fields with a center (classified as ON or OFF depending on whether the neuron increases its firing rate to an increase or decrease in luminance at the center) and an antagonistic surround (which is larger than the center and has luminance preference opposite to that of the center). Center-surround antagonism is also found in other sensory modalities such as in the auditory periphery [Knudsen and Konishi, 1978], in the somatosensory cortex [DiCarlo et al., 1998], and in the whisker barrel system [Bellavance et al., 2010, Simons and Carvell, 1989].

Early theories about the function of center-surround antagonism include edge enhancement [Hartline et al., 1956] and redundancy reduction [Attneave, 1954, Barlow, 1961]. Testing and extending these theories remains an active experimental and theoretical field [Atick, 2011, Dan et al., 1996, Kuang et al., 2012, Ol-

shausen and Field, 1996b, Pitkow and Meister, 2012, Puchalla et al., 2005, van Hateren, 1992, Atick and Redlich, 1992, Graham et al., 2006].

The computational effect of surround antagonism depends on the relative strength and size of the center and surround. For example, weak surrounds achieve low-pass spatial frequency filtering and are optimal for de-noising when signal-to-noise ratio (SNR) is low, while balanced surrounds achieve band-pass spatial frequency filtering and are optimal for de-correlation of responses when SNR is high [Atick and Redlich, 1992]. The strength and size of both the center and surround of the receptive fields of neurons in the retina and the dLGN has been measured in multiple species [Alitto et al., 2011, Cheng et al., 1995, Dacey et al., 2000, Grubb and Thompson, 2003, Heine and Passaglia, 2011, O'Keefe et al., 1998, Xu et al., 2002]. These studies all find a distribution of surround strengths ranging from weak to balanced, with an average surround about 75% the strength of the center.

Rodents are becoming an important model to study visual circuits due to their availability and relative inexpensiveness, their ability to perform complex behaviors [Busse et al., 2011, Creer et al., 2010, Harvey, 2012, Meier et al., 2011, Zoccolan et al., 2009], their applicability to studying visual diseases [Sekirnjak et al., 2011] and the relative ease of applying genetic techniques [Morozov, 2008, Thomas and Capecchi, 1987] to modify circuit function. The functional properties of the early visual system of rodents have been characterized since the 1960s [Anderson and Yoshida, 1977, Fukuda et al., 1979, Kriebel, 1975, Lennie and Perry, 1981], but the strength of surround antagonism has not been studied in detail.

2.2 Experimental Procedures

All procedures were conducted with the approval and under the supervision of the Institutional Animal Care and Use Committee at the University of California San Diego. Six male Long-Evans rats (Harlan) were used for this study. A preliminary account of these physiology methods, including surgical implant design, head fixed recording methods, integration with stimulus display and eye-tracking hard-

ware and software, has been presented previously [Flister and Reinagel, 2010, Sriram et al., 2011].

2.2.1 Surgery

Adults hooded male rats (Rattus norvegicus, >P90) are deeply anesthetized using 5% isoflurane. Ringers solution (15 ml/kg) is provided for hydration and Atropine (0.05 mg/kg) is injected to control secretion. The scalp is shaved and sterilized with 70% isopropyl alcohol/Betadine pads. The rat is placed on a stereotaxic apparatus and Sensorcaine (0.1 ml) injected into the scalp. An incision is made over the left dLGN (4.5mm Posterior, 3.5mm Lateral from Bregma). After removing the fascia over the skull, a craniotomy is drilled over the putative dLGN center (dimensions: 1.5-2 mm M-L, 2-3 mm A-P). An eppendorf tube is glued over the craniotomy to provide easy access for future recording. Titanium screws (5 or 6) are placed over the exposed skull and the craniotomy filled with cement. A hex standoff and an aluminum spacer are also included in the head cap for future head fixing.

2.2.2 Head-fixing rats

Male rats are constrained in a sock and injected with a mild sedative, Midazolam (0.3-0.6 ml/kg), 10 minutes prior to being placed on the rig. Rat's heads are fixed with screws threaded through the standoff and the spacer. In our hands, this led to stable recording sessions lasting about 120 minutes and allowed for stable recording of single units lasting 10-20 minutes in duration. Each rat can be used for recording for a duration between 3-12 weeks.

2.2.3 Stimulus presentation

One of two monitors (Westinghouse L2410NM(LCD)/Sony Trinitron PF790-VCDTS21611(CRT)) was used to present visual stimuli. Results were similar in the recordings collected with both monitors. Both monitors were empirically linearized, and all stimuli were presented at a frame rate of 60 Hz, and a mean

luminance of 25 $cd.m^{-2}$. The monitor was placed at a tangent 30cm (LCD) or 20cm (CRT) from the rat's right eye, such that the display filled at least $85° \times 60°$ of visual field in both cases. Simultaneous with each frame update, a 5V synchronizing TTL pulse was sent to the recording computer (see below). Frame drops often occurred in the first few frames of the trial; we used only the data after any such frame drops. If any frames were dropped later in a trial, the entire trial was excluded from analysis. Our stimuli were constructed using the Psychophysics toolbox [Brainard, 1997, Pelli, 1997, Kleiner et al., 2007]. Custom Matlab (Mathworks Inc., Waltham, MA) scripts were used to present either stochastic noise stimuli or drifting gratings stimuli to the right eye of the rat [Meier et al., 2011].

2.2.4 Electrophysiological recording

The chronic well was exposed, and an extracellular electrode (Tungsten, FHC, Bowdoin, ME or pulled Quartz microelectrodes filled with ringers solution) was inserted stereotaxically to defined coordinates (4.5P,3.5L,5-6V) in the rat brain. Voltage traces were amplified (10-1000X) and filtered (1Hz-10kHz) (AM1800; AM Systems, Sequim, WA), digitized (NIDAQ PCI-6259, National Instruments, Austin, TX), and stored in a local computer. Synchronizing TTL pulses from the stimulus computer were recorded simultaneously on a separate channel. After each session, the well was washed well with antibiotic solution (Baytril 0.05mg/ml), cleaned well with neutral saline and plugged with silicone gel until the next session.

The subjects in this study were unanesthetized but were not performing any visual task, and we did not record an EEG. Therefore we cannot know if the rats were "alert". We monitored, however, for two indirect signs of drowsy/inattentive state: (1) eyelids partially or fully closing, as observed by the infrared eye tracking camera; or (2) dLGN neurons entering a rhythmic bursting firing mode. In this same preparation it was previously shown [Flister and Reinagel, 2010] that this rhythmic firing mode in the dLGN is accompanied by an increase in synchronous power in the alpha band of the LFP, and is comprised of bursts that resemble the low-threshold Calcium bursts often associated with sleep and anesthesia in

other species. If or when the rat appeared drowsy or inattentive by either of these criteria, we used mild stimuli (clapping hands, gently brushing tail, squirting water in mouth) to arouse them, or ended the recording session if these measures were ineffective. Post-hoc analysis confirmed that bursts were mostly absent from our recorded data.

2.2.5 Single Unit Isolation

Single units were identified as negative (tungsten,FHC) or positive (quartz microelectrode) deflecting spikes of much larger amplitude than noise or any other spikes (e.g., see Figure 2a). Rough sorting criteria were used to characterize the single unit during the experiment. All analyses shown were performed on more stringent offline sorting using Klustakwik [Harris et al., 2000]. Units were kept for analysis if they met several criteria: (1) thresholded spike waveforms were aligned at the positive peak and all waveforms formed a well isolated cluster; (2) spike shape was relatively constant; and (3) no refractory violations. Spike amplitude variation was common for well-isolated single units, depending on the preceding inter-spike interval. Care was taken to include as many of the spikes as possible despite this amplitude variation.

2.2.6 Eye tracking

The rat's eye position was monitored using an infrared tracker (Eyelink 1000, SR Research, Kanata, Ontario, Canada). Clear artificial tears were applied to the eyes to keep them moist. Excess tears were removed using a cotton swab. Tracking data was digitized using the EyeLink Toolbox [Cornelissen et al., 2002]. When stimulated by noise or touch (see above), rats make low-amplitude ($< 5°$) saccades [Hikosaka and Sakamoto, 1987] (but see [Chelazzi et al., 1989]). In our preparation, these saccades are infrequent (<1 Hz) at the time stimuli occur, and even less frequent when the rat is undisturbed. After saccades, the eye position typically decayed back to the central fixation point. Preliminary experiments showed that in our preparation rats maintain fixation within a 5° circle around the mean

eye position >65% of the time and within 15° > 95% of the time (data not shown).

The stability of eye position was sufficient for us to ensure the receptive field remained within the full-field grating stimulus for the duration of the recording. But eye movements could affect the phase of the grating relative to the receptive field for all but the lowest spatial frequencies probed (see for example the rasters in Figure 2c). Thus we do not report the absolute phase of the stimulus in our analysis. We used drifting (not counterphase) gratings, and computed the neuron's response independently each trial (see below), such that phase differences from trial to trial would not affect our measure of the amplitude of the response.

2.2.7 Single Unit Characterization

Once single units were identified as visually driven (using an opthalamoscope) the position of the rat relative to the monitor was adjusted such that the receptive field of the unit was within the extent of the monitor. White noise stimuli were used to locate the center of the receptive field within the monitor when eyes were at the mean eye position. Once the location of the receptive field was identified, vertical drifting gratings of varying spatial frequencies was presented to the rat on a linearized CRT monitor. Gratings were at full contrast and drift frequency was 2 or 4 Hz with a frame rate of 60 frames/s. This drift frequency was chosen so as to drive maximal neural responses without engaging the Optokinetic Reflex (Fuller 1985; our unpublished observations). Each 'trial' consisted of a 2 or 3 s presentation of a constant spatial frequency; spatial frequencies were interleaved in pseudorandom order without gaps between until each stimulus was presented once, and this sequence was repeated three or more times.

2.2.8 Spatial Frequency Tuning

The responses of each single unit were temporally discretized at the stimulus refresh rate (60 Hz). To mitigate the effects of small eye movements on stimulus phase, response power estimates were calculated on a trial by trial basis as the Fourier transform of the autocorrelation function (Wiener-Khinchin theo-

rem). This was repeated for each trial for a specific spatial frequency and across all spatial frequencies. The f1 response amplitude for each trial was measured as the square root of the power at the stimulus temporal frequency. Care was taken to ensure that the measured amplitude actually corresponded to a peak in the spike train power spectrum. If no peaks were visible, the single unit was rejected from the analysis. Non-stationary units, showing inconsistent tuning curves or large changes in mean rate between repeats, were rejected from the analysis. To further estimate the significance of the measured amplitudes, a resampling approach was taken. The spike train from each repeat was shuffled while maintaining the inter-spike interval distribution. The power of the resampled spike trains was calculated using the methods described earlier. A 'virtual' experiment involving these reshuffled spike trains were then used to estimate the noise floor at each spatial frequency. This shuffling process was repeated multiple (100) times to obtain a mean noise floor as well as the SD of the noise floor at each frequency. While the calculated f1 values were indistinguishable from the noise floor at some (especially high) spatial frequencies, in all the units included, contained responses at multiple spatial frequencies where the mean actual f1 response was more than 2 SDs from the estimated noise floor mean.

2.2.9 Fitting DOG Model

Custom MatLab routines were used to fit f1 responses with a modified difference of Gaussians (DOG) model [Enroth-Cugell and Robson, 1966, Grubb and Thompson, 2003]:

$$R_\nu = \mathcal{S}\left(R_\nu\right) + \| K_c \pi r_c^2 e^{-\pi^2 r_c^2 \nu^2} - K_s \pi r_s^2 e^{-\pi^2 r_s^2 \nu^2} \| \tag{2.1}$$

$$r_c < r_s;\ K_c > K_s$$

The calculated shuffle estimates $\mathcal{S}\left(R_\nu\right)$ were subtracted from the actual response to eliminate the residual power present in the spike train not associated with the stimulus. The absolute value function is used because the measured power

is constrained to be positive. The Simplex Search Algorithm (`fmincon` in Matlab) was used to search for the correct combination of parameters (K_c, K_s, r_c, r_s) that best fit the response under a constrained optimization protocol. For each single unit, fitting was done to three separate non-linear constraints:

$$\eta < 1, \eta = 1, \eta > 1$$

where

$$\eta = \frac{K_s r_s^2}{K_c r_c^2} \tag{2.2}$$

is the ratio of the integrated weight in the surround to the integrated weight in the center [Xu et al., 2002, Croner and Kaplan, 1995, Enroth-Cugell and Robson, 1966, Grubb and Thompson, 2003]. This provided three separate classes of solutions to which each single unit belonged. The fitting algorithm minimized the sum of the squares of the difference between fitted values and the actual values (2.3).

Because of the nature of the fitting algorithm and due to the presence of noise in the data, there is no guarantee of discovering the global minimum of the cost function. We ensured good fit by repeating the fitting process multiple (n = 100) times with random initial guesses. The quality of each of these fits was evaluated based on the Pearson correlation between the actual data and data from fits. The highest quality fit within each constraint was chosen as the candidate fit for that class of solutions. From the three candidate solutions, the final solution was taken to be the one which had the highest quality fit, except that solutions with $\eta > 1$ (surround stronger than center) were rejected if a solution with $\eta = 1, \eta < 1$ fit equally well (quality of fit within 2%). Thus we were conservative with respect to our claim that surrounds can be stronger than centers.

2.2.10 Histological confirmation of recording sites

Each subject was recorded in multiple sessions over 3-12 weeks. At the final recording session, an injection syringe loaded with 2% pontamine sky blue

solution was lowered to the stereotaxic coordinates of the last recorded unit as a fiduciary mark for histological analysis. The subject was euthanized, perfused, and the brain tissue fixed, sectioned, and examined. In all cases we confirmed that the stereotaxic coordinates of the recording sites of our single units fell within the boundaries of the histologically identifiable dLGN [”Discenza, 2011, ”Paxinos and Watson, 2006].

2.3 Results

In order to estimate the surround strength of the receptive fields we employed a standard method of fitting the spatial frequency response of a unit to a difference-of-Gaussians (DOG) model [Enroth-Cugell and Robson, 1966, Grubb and Thompson, 2003].

We recorded 83 well isolated single units in the putative dorso-lateral geniculate nucleus of unanesthetized head-fixed rats while they passively viewed drifting high contrast (100%) sinusoidal gratings on a linearized CRT/LCD monitor with a mean luminance of 25 $cd.m^{-2}$. The monitor was approximately centered on the cell's receptive field and filled $85^\circ \times 60^\circ$ of visual field. We varied the spatial frequency of the grating from $0.02 - 0.36$ $cyc/^\circ$ $(50 - 3\ ^\circ/cyc)$, keeping the temporal frequency constant at 2 or 4 Hz. We only include in subsequent analysis the cells whose spatial receptive field center was clearly within the confines of the monitor as measured using the spike-triggered-average to a white noise stimulus [Chichilnisky, 2001], and whose responses were stationary (see Methods). Of the 83 recorded 47 fit the criteria. The recording locations were later confirmed histologically.

2.3.1 Responses in unanesthetized rat dLGN to drifting gratings

Responses of one representative OFF cell are summarized in 2.4. The raw voltage trace in response to a drifting grating for one 3-s trial (2.4a) shows the quality of isolation of the unit, and reveals that the firing rate was modulated over time by the stimulus (2.4b) at this spatial frequency. The drift speed was

adjusted such that the temporal frequency of modulation was the same for all spatial frequencies. The responses to all repeats of all spatial frequencies are summarized by rasters grouped by spatial frequency (2.4c).

For the cell shown, the mean firing rate depended on spatial frequency (Figure 2.5a), as was the case for N=36/47 cells in our population. The highest mean rate for any spatial frequency was 68 spikes/sec for this cell, and 22.89 ± 11.27 spikes/sec (mean±SD) across our population. This cell showed response modulation at the temporal frequency of the stimulus (2Hz) (Figure 2.5b), which reflects the linear component of the response. At its optimal spatial frequency (chosen by the peak of f1), modulation of this cell was 77% of the mean rate ($\frac{f1}{f0}$). All cells in our sample were well modulated at their optimal spatial frequency: $\frac{f1}{f0} = 0.66 \pm 0.15\%$ (mean±SD across the population).

This cell also had some response power at twice the input temporal frequency (f2, Figure 2.5c). This weak f2 response is attributable to rectification and rebound, but does not resemble a classic frequency-doubling response typical of Y cells (Hochstein and Shapley 1976a; b). Although no detailed cell classification has been attempted, we refer to this cell as "X-like" merely to indicate that at the optimal spatial frequency, $\frac{f2}{f1}$ (=0.41) was less than unity. By this definition 46/47 of the cells in our sample were X-like (Figure 2.5d).

2.3.2 Measuring Surround Antagonism

A standard method for measuring the extent of surround antagonism is a difference of Gaussian (DOG) model fit from spatial frequency tuning curves [Grubb and Thompson, 2003]. We used the linear response to the grating (f1, see Figure 2.5b) to fit the spatial receptive field center and surround components (see Methods). For the example cell shown in Figures 2 and 3, the best fit DOG model (Figure 2.6a) had a center radius r_c of 4°, and a surround radius r_s of 13°, and a relative surround strength of $\eta = 0.83$. This is typical low-pass tuning curve in our sample, and this type of response is well described in the literature. A DOG receptive field with a weak surround relative to center is consistent with strong response modulation even at the lowest spatial frequencies tested.

The measured tuning curve of another example cell is shown in Figure 2.6b, along with the fit obtained from the best DOG model. This is a typical band-passed tuning curve: responses fall off at both high and low spatial frequencies. This cell's receptive field model had a center radius r_c of 2.19°, and a surround radius r_s of 3.75°, and a relative surround strength of $\eta = 1$. A DOG receptive field with a well-balanced surround relative to center is consistent with lack of response to low spatial frequencies, and is well described in the literature.

We also found a third type of tuning curve in our sample (Figure 2.6c) which has not been well described previously (but see [Heine and Passaglia, 2011]). These spatial frequency tuning curves could be described as dual-band-pass or notched; the notch occurred at different spatial frequencies for different cells. While DOG models with balanced ($\eta = 1$) or weak ($\eta < 1$) surrounds could not reproduce these tuning curves, they were easily fit by DOG models with strong surrounds ($\eta > 1$). This cell's receptive field model had a center radius r_c of 2.00°, and a surround radius r_s of 3.97°, and a relative surround strength of $\eta = 2.2$. Interpretation of these cells will be considered further in the discussion.

We measured the integrated weight of the surround relative to the center by the variable η (Equation 1, Methods). In our data values of η ranged from $\eta = 0.02$ to $\eta = 80$ (Figure 2). The value of η corresponded closely to the shape of the spatial frequency tuning curve. All cells that showed significant fall-off of the response at low spatial frequencies had η values close to 1 (Figure 2.6b). Those that showed little fall-off at low spatial frequencies had η values less than 1 (Figure 2.6a), and all cells that showed notched spatial frequency tuning curves had η values greater than 1 (Figure 2.6c).

The majority of cells (N=29/47) had well balanced center and surround with $0.95 \leq \eta \leq 1.05$. Several (N=8/47) had weak surrounds ($\eta < 0.95$) as previously described in other studies. A substantial fraction of cells (10/47) had values $\eta > 1.05$, indicating a surround that is stronger than the center. Because this result was unexpected, our analysis was conservative in assigning fits with $\eta > 1$: we searched separately for the best fit model with $\eta = 1$ and with $\eta < 1$, and chose one of these solutions preferentially if the fit was almost as good (see

Methods). We emphasize that this reflects the integrated weight of the center and surround over space, and the surround radius was often much larger. The peak sensitivity of the surround K_s was less than that of the center K_c in all cases.

2.4 Discussion

We have used spatial frequency tuning to estimate the spatial structure of receptive fields in the dLGN of unanesthetized rats. The distribution of receptive field center sizes we find is in good agreement with that previously reported for retinal ganglion cells of the rat [Heine and Passaglia, 2011]. Some neurons in our sample had weak surrounds, as reported in other species. We find that most dLGN neurons in the unanesthetized rat, however, have well-balanced surround antagonism and thus a band-pass rather than low-pass spatial frequency tuning. This differs from the distributions reported in other species, in which surrounds are typically weaker [Cheng et al., 1995, O'Keefe et al., 1998, Xu et al., 2002]. The distribution of surround strength has not previously been reported in either anesthetized or unanesthetized rodents. In anesthetized mouse dLGN, both low-pass and band-pass spatial frequency tuning curves have been observed [Grubb and Thompson, 2003] consistent with receptive fields ranging from weak to balanced. In optic nerve recordings in anesthetized rats, retinal ganglion cell spatial frequency tuning curves were found to be mostly low-pass, although band-pass tuning curves were also observed [Heine and Passaglia, 2011].

We also report several examples of cells with unexpected, notched or dual-band-pass tuning curves which have not been reported in other species (but see Figure 7 in [Heine and Passaglia, 2011]). These data could be well fit by the standard circularly concentric DOG model if the integral of the surround component exceeded that of the center (Figure 2.6c). For an intuition, consider a set of model cells with center size 1°, surround size 3°, and different surround strengths. Figure 2.8 shows the response of such model cells to drifting gratings, separated into center and surround components. The center response (C) and the surround responses (S) are both decreasing functions of spatial frequency. As the surround strength

increases, the response at the lowest spatial frequency for center and surround get closer in value. The net response at lower frequencies (C-S) diminishes. For the case where the surround is stronger than the center, the net response (C-S) reaches zero at an intermediate spatial frequency and takes negative values, corresponding to a phase reversal in the grating response. However, the value that is experimentally measured is the amplitude of the response modulation about the mean, which is always a positive value. Therefore when center and surround responses are summed, a notched or dual-band-pass tuning curve is produced. We take this to be a simple and conservative explanation of the data, though other models are possible, such as an antagonistic surround that is spatially offset relative to the receptive field center (Soodak 1986). Regardless of how these tuning curves arise mechanistically, such cells clearly do occur in our data.

2.4.1 Linearity of Responses

Difference-of-Gaussian models based on spatial frequency tuning data are widely used to describe spatial receptive field structure of both X and Y cells in the retina and dLGN [Bonin et al., 2005, Linsenmeier et al., 1982, Sceniak et al., 2006]. If the combined circuitry leading from the visual image to a dLGN neuron's response were a perfectly linear system, response due to the center and surround components to an arbitrary pattern of light would be separable and add linearly, and this method of measurement would be exact. To the extent that responses in the dLGN are nonlinear, this method provides only an approximation or a description of the linear component of the response. Not surprisingly, past studies report that better fits are obtained for X cells than for Y cells [Linsenmeier et al., 1982].

For the cells in our study we do not have data from standing phase reversing gratings or sparse noise, which would be required to determine whether the receptive fields contained nonlinear spatial subunits. Based on the ratio of the f2 to f1 responses to drifting gratings, most of the neurons in our population had relatively linear responses. In this specific sense, we refer to our cells as 'X-like' (Figure 2.5d), and we find our data to be well fit by the DOG model. We note that

additional classes of neurons in the dLGN with other response properties, including nonlinear or Y-like cells, might exist but could be missed due to an unknown selection bias in our recording technique.

Another known form of nonlinearity in the dLGN is extra-classical surround suppression, which is modeled as a divisive normalization component [Bonin et al., 2005, Heeger, 1992]. Our drifting grating stimuli were large compared to the classical receptive field centers, and therefore may have engaged extraclassical surround suppression. Indeed we find that responses in the dLGN can be sensitive to the size of the stimulus aperture (our unpublished data). Divisive normalization, if present, would affect the absolute amplitude (K_c,K_s) of our DOG fit but should not impact our measures of center or surround radius (r_c, r_s) nor the relative sensitivity ($\frac{K_s}{K_c}$) or surround strength (η).

2.4.2 Location of computation

We have measured center-surround antagonism in the dLGN of the unanesthetized rat. This property is at least partly inherited from the retinal inputs to the dLGN. We do not have access to a comparable measurement of surround strength in rat retinal ganglion cells, so it remains to be determined if thalamic or cortico-thalamic circuitry contribute to surround strength in the dLGN of the unanesthetized rat. In other preparations, however, surrounds of dLGN receptive fields are thought to be stronger than that of their retinal inputs [Cheng et al., 1995, Hubel and Wiesel, 1961]. Anesthesia is known to affect dLGN responses; we cannot exclude the possibility that anesthesia affects surround strengths in the dLGN.

2.4.3 Computational Function

Our results imply that in the unanesthetized rat, most cells in the dLGN are transmitting a signal that is spatially decorrelated, and therefore less redundant and more sparse than the luminance patterns found in natural scene scenes [Barlow, 2001, Olshausen and Field, 1996b, Olshausen and Field, 1996a]. It remains unclear

whether the resulting compression of the image is the most important function of this spatial filtering operation, given that the combined effect of eye movements already tends to spatially decorrelate or 'whiten' the image prior to encoding by photoreceptors, at least in some species [Reinagel and Zador, 1999, Kuang et al., 2012]. Alternatively, the function may be primarily the enhancement of edges: well-balanced surround antagonism would maximally enhance the difference between inputs to ON and OFF subregions of V1 receptive fields along edges and contours, serving to facilitate edge detection.

A smaller population of cells had notched or dual-band-pass spatial filters, which can be explained by extra-strong surrounds in the classical center-surround receptive field. This property may be inherited from retinal ganglion cells [Heine and Passaglia, 2011]. It remains to be determined whether these unusual tuning curves are a functional adaptation to visual coding, or merely a consequence of imperfect wiring. In either case, this response type comprises a substantial fraction of our sampled population, so it will be important to determine their impact on the neural code of the rat dLGN.

Another subpopulation of cells in our sample had weak surround antagonism, as widely reported in other species. These cells carry a smoothed image representation that would be spatially correlated for natural images, with little or no edge enhancement. Perfect surround antagonism removes all information about absolute luminance from the image representation; a small subset of neurons with weak or absent surrounds would be sufficient to carry this complementary information.

We find heterogeneity of surround architecture in the dLGN population, which may be functionally important [Soo et al., 2011]. Past theories derived the optimal surround strength for a homogenous population of units under different stimulus conditions; it would be interesting to extend this approach to consider optimal distributions in a heterogeneous population.

Chapter 2, in part, has been submitted for publication of material as it may appear in Journal of Vision, 2012. The dissertation author is the primary investigator and the first author of the paper.

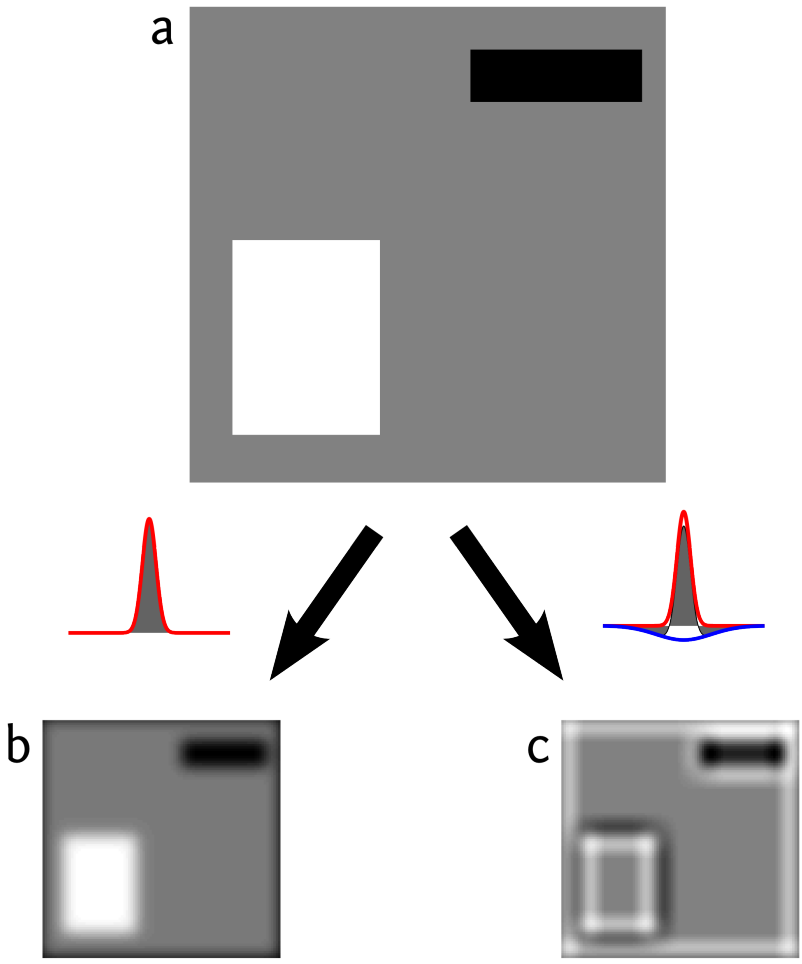

Figure 2.2: **Response profile of a bank of filters to edges.**
a Shows an image with both light and dark edges. **b** is the response profiles of a bank of neurons having only a center-subunit. Edges look blurrier than in the image **a**. However, the filter in **c** includes a surround and the responses of bright edges are enhanced, while the responses of dark edges are unaffected. To enhance dark edged one would need an OFF-center filter.

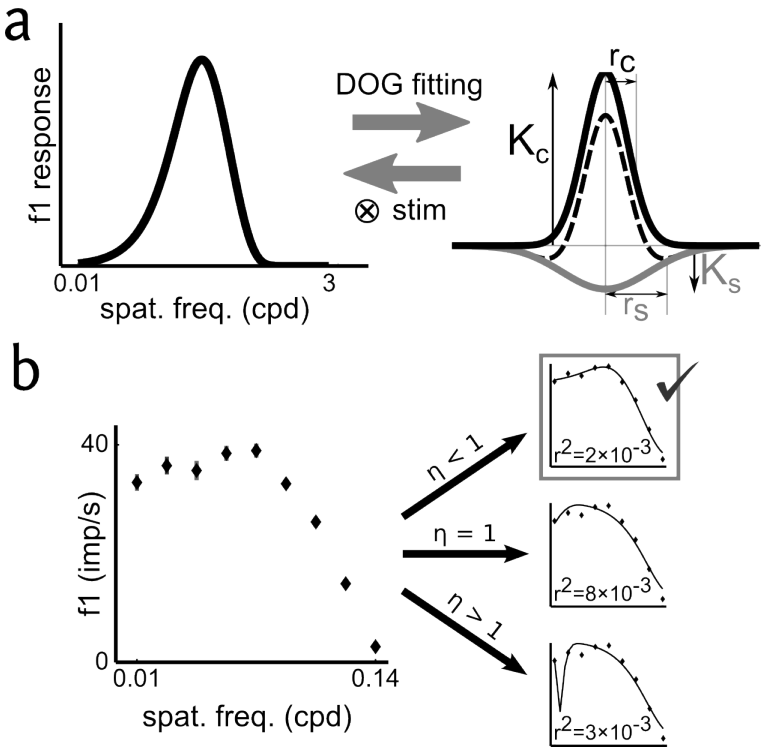

Figure 2.3: **Difference of Gaussian Model Fitting.**
a A model receptive field is defined by two circular, concentric 2D Gaussian densities, a cross section through which is shown at right. The receptive field center (solid black curve) is defined by the radius r_c and peak amplitude K_c of the smaller Gaussian, the sign of which determines the response type (ON or OFF) of the model neuron. The classical surround (solid gray curve at right) is defined by the radius r_s and peak amplitude K_s of the larger Gaussian. The model receptive field is the linear sum of these components (dashed curve). The predicted spatial frequency tuning curve for a DOG model is obtained by convolving sinusoidal gratings of different spatial frequencies with the spatial receptive field. Alternatively, the receptive field sensitivity profile of a recorded neuron may be estimated by fitting the DOG model parameters to optimize the match to the observed spatial frequency tuning responses (SEE METHODS). **b** Each neuron's tuning curve (example cell at left) was fit to the best DOG model receptive field under three separate constraints: $\eta < 1, \eta = 1$ *and* $\eta > 1$ (SEE METHODS). The predicted tuning curves (thin curves, right) were compared with the data, and the solution having the highest quality of fit (least r^2) was selected as the best model for that cell.

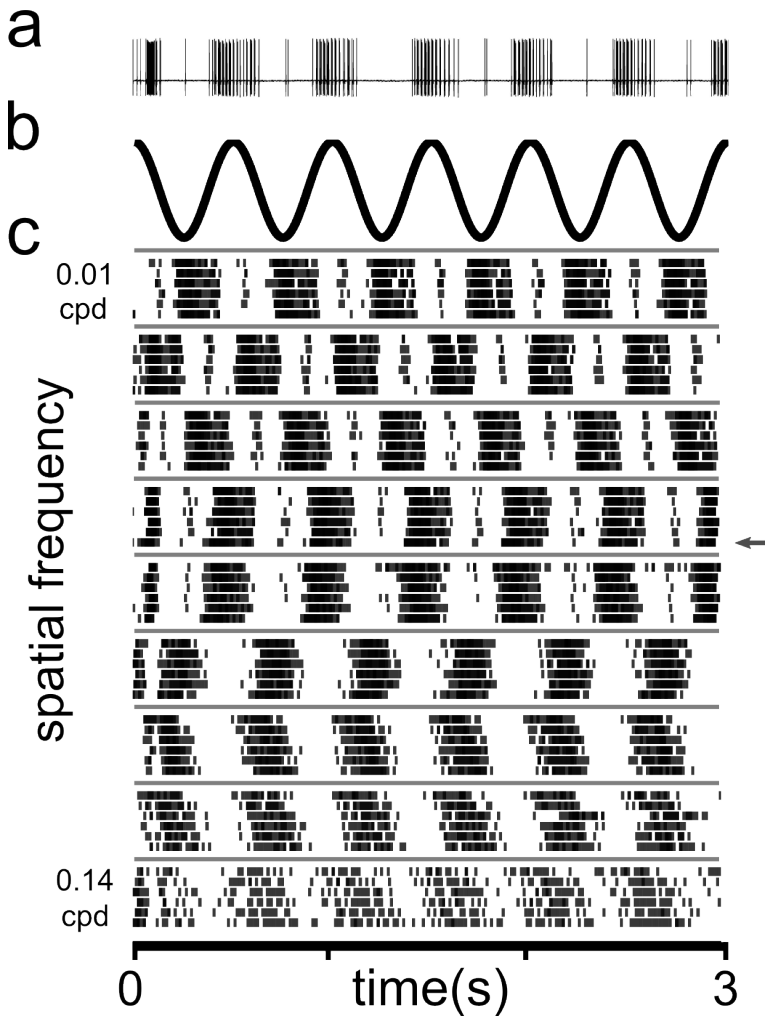

Figure 2.4: **Responses to drifting gratings.**
a High-pass filtered voltage trace from one single unit recorded from the dLGN of an unanesthetized rat. The raster corresponding to this trial is marked with an arrow in **c**. **b** Stimulus luminance at an arbitrary point on the display. Temporal frequency was 2 Hz, for six complete cycles within the 3 second duration of a trial, regardless of spatial frequency. **c** Rasters for this single unit obtained for all spatial frequencies, where each row indicates responses for a single trial and each tic mark indicates the time of a single action potential. The six trials recorded at each spatial frequency were interleaved during the experiment but are grouped by spatial frequency for display. The time axis at bottom applies to all panels.

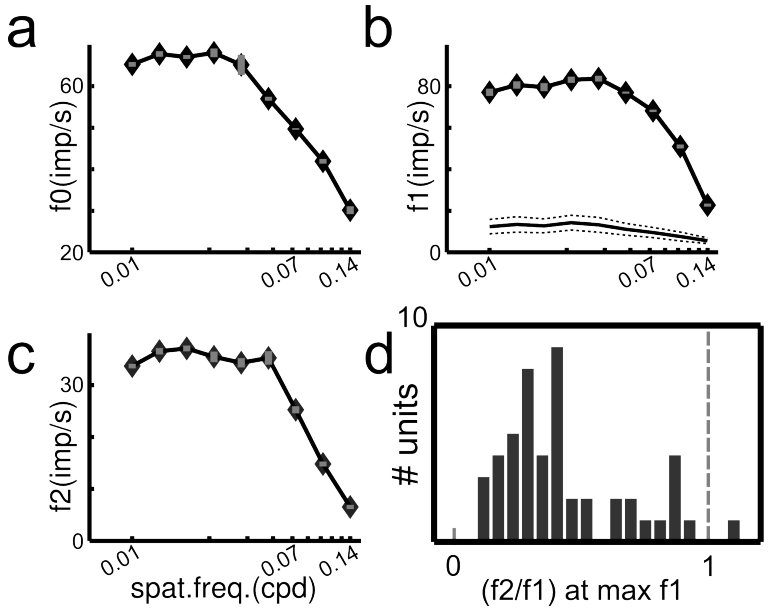

Figure 2.5: **Spatial frequency tuning analysis for an example cell.**
a Average firing rate (f0, in impulses per second) as a function of spatial frequency (shown on a log scale), for the data shown in Figure 2. Diamond symbols show the mean obtained over trials, error bars (gray) show the standard error of the mean (SEM) across trials. **b** Modulation in firing rate about the mean, at the temporal frequency of the visual stimulus (f1 = 2Hz). **c** Modulation of the firing rate at twice the stimulus frequency (f2 = 4Hz). Dashed line in (a),(b) and (c) indicates the spatial frequency at which the f1 response is highest (peak in 3b). Values of f2 and f1 at this spatial frequency were used to compute the ratio f2/f1, which for this cell is 0.17. A ratio > 1 indicates frequency doubling, a nonlinear characteristic of Y-like cells. **d** Distribution over the population of cells of the f2/f1 ratio measured at the spatial frequency with maximum f1 response.

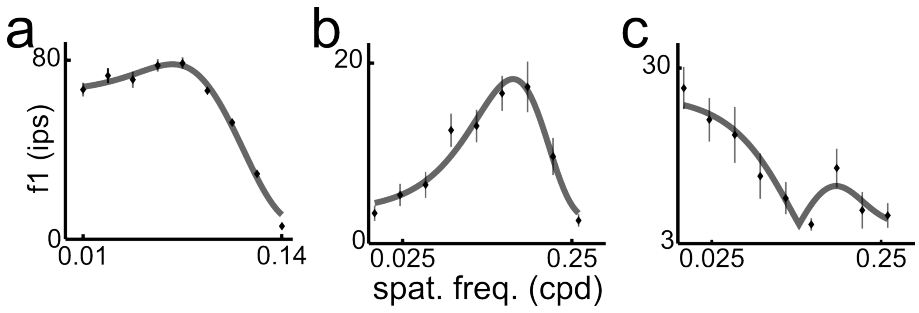

Figure 2.6: **Three classes of spatial frequency tuning curves.**
In each panel, the f1 response for one recorded neuron is shown as the mean f1 over trials (diamonds) +/- SEM across trials (thin gray lines), as a function of spatial frequency (cycles per degree) on a log scale. The tuning curve predicted by the best-fit DOG model receptive field is overlaid (thick gray curve) in each case. **a** Spatial frequency tuning curve for an example low-pass tuned cell. **b** Spatial frequency tuning curve for an example band-pass tuned cell. **c** Spatial frequency tuning curve for an example notched or dual-band-pass cell.

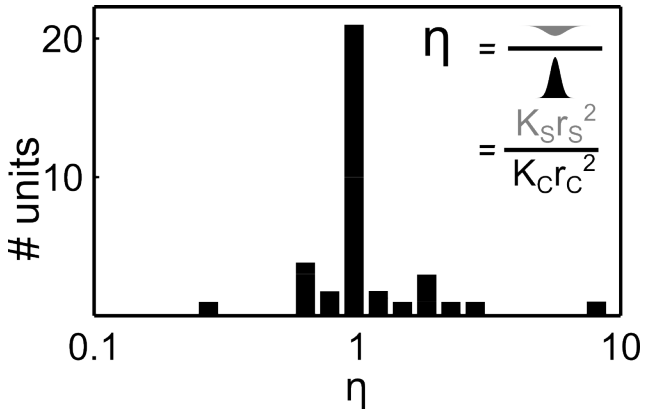

Figure 2.7: **Distribution of η.**
The integrated strength of the surround relative to the center is given by η (inset equation). The distribution of η (shown on log scale) over the population is shown. The data are clustered near $\eta = 1$, corresponding to well-balanced surround strength. Units with weak surrounds are at left ($\eta < 1$), while those with stronger-than-balanced surrounds are at right ($\eta > 1$).

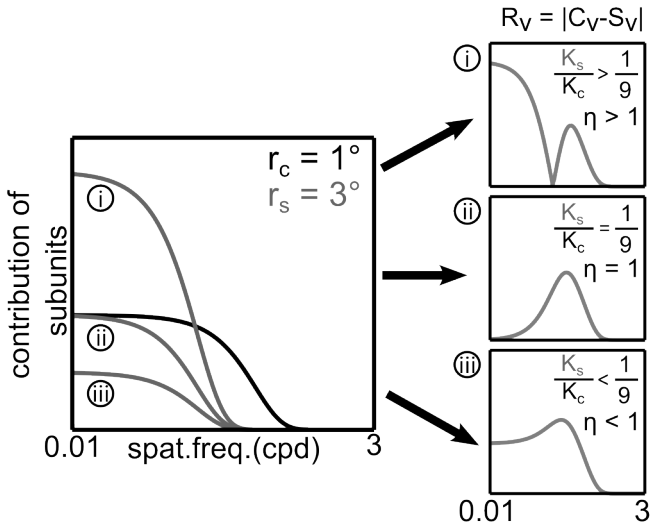

Figure 2.8:
Intuition for notched or dual-band-pass tuning curves. Responses of the center and surround components to drifting gratings of different spatial frequencies for three hypothetical cells (left). Center response (black curve) is for a Gaussian profile with radius r_c of 1° and arbitrary sensitivity of 1, and is the same for all three model cells. Surround responses (grey curves) are for Gaussian profiles with r_s of 3° and different sensitivities relative to the center. When the integrated surround strength is less than that of the center (iii), the response reaches a plateu at low spatial frequency. When the center and surrounds balance (ii), response falls to 0 at low spatial frequency. If the surround response exceeds that of the center (i), a node in the tuning curve results.

Chapter 3

Modeling Classical and Non-Classical Surrounds

Receptive fields in the early visual system are thought to have at least two functionally separable types of surrounds. Classical surrounds were discussed in Chapter 2. In this Chapter, I examine the evidence for the presence of Non-Classical Surrounds by identifying features not explained by the simple classical surround, identify models that capture these features and discuss the practical implications of measuring these surrounds.

3.1 Existence of a Non-Classical Receptive Fields

The linear, spatial receptive field model(explained in Chapter 2) along with its temporal component can be used to predict many features of neuronal responses in the early visual system: responses to dots of light, the size and timing of spiking responses to gratings of varying spatial and temporal frequencies [Cai et al., 1997, Dawis et al., 1984] and in some cases, even to predict responses to complex noise stimuli [Keat et al., 2001]. However, it was less successful in predicting responses to certain simple stimuli quantitatively or to predicting responses to complex, naturalistic stimuli even qualitatively. Over the years a number of signatures response properties of non-classical receptive fields have been identified:

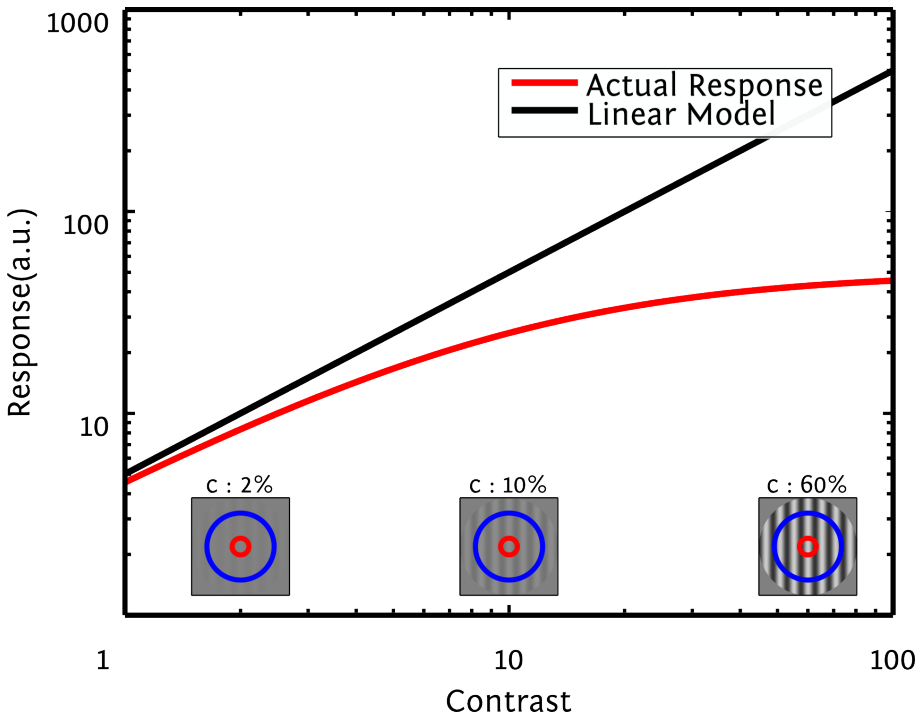

Figure 3.1: **Contrast Saturation.**
Linear model predicts larger responses at high contrasts compared to actual responses. Responses of a linear model is shown in black whereas the responses of actual neurons (red curve) level off at higher contrasts.

- **Responses Saturate at High Contrasts:** A linear model predicts that the response scales linearly with contrast. However, responses of neurons in the early visual system saturates at high contrasts, often at firing rates far below the maximal possible firing rate.[Maffei and Fiorentini, 1973, Sclar et al., 1990, Bonin et al., 2005]

- **Size Tuning:** Neurons in the dLGN are tuned to the size of the stimulus. This is typically measured by measuring the responses of neurons to gratings of increasing sizes. Responses peak at an intermediate aperture radius and then fall to a lower value as the aperture radius increases. The fractional reduction in responses for large stimuli compared to the maximal response is defined here as the Suppression.

- **Size Dependent Response Reduction is Contrast Dependent:** Responses of neurons to drifting gratings of increasing size show substantial

suppression in responses for high contrast with little or no suppresion at lower contrasts [Jones et al., 2000, Jones and Sillito, 1991, Bonin et al., 2005, Solomon et al., 2002]. A linear model however predicts identical suppression at all contrasts.

- **Increase in Optimal Response Radius is Contrast Dependent:** At low contrasts, the peak response radius as estimated from size tuning curves shifts to higher values [Nolt et al., 2004]. Linear models predict no shift in the peak response radius.

Apart from the above features, which will be considered in full by this Chapter, other features have been observed both within the dLGN as well as in the Retina and Visual Cortex(V1) which indicate the presence of a non-classical surround. In particular, a region of the receptive field called the Extra-Classical Receptive Field has been identified. This Extra-Classical Receptive Field is thought to be an area where stimuli do not themselves drive the responses of the neuron under consideration, but modulate the responses to stimuli within the classical receptive field. Due to its very definition, this area has been located far away from the classical receptive field, often extending upto three times the radius of the classical receptive field [Levick et al., 1972, Murphy and Sillito, 1987, Alitto and Usrey, 2003] (but see [Bonin et al., 2005]). Extra-classical receptive fields of neurons are known to be orientation tuned in V1 [Cavanaugh et al., 2002b, Cavanaugh et al., 2002a, Sillito et al., 1995] and are thought to be dependent on the difference in orientation between center stimulus and surround stimulus in the dLGN [Sillito et al., 1993]. Both of the above facts were discovered in experiments involving masking. Furthermore, neurons in V1 show Cross-Orientation Suppression - a phenomenon where superimposition of additional gratings onto the receptive field centers of V1 a neuron suppresses its response[Morrone et al., 1982]. These effects, though well described in the literature will not be considered further.

3.2 Models of Classical and Extra-Classical Receptive fields

A variety of approaches have been taken to understand Non-Classical receptive fields' effect on Classical receptive field responses. They range from descriptive approaches, to models incorporating the non-classical receptive field as a linear component to the actual receptive field [Alitto and Usrey, 2005, Sceniak et al., 2006], to more complex and realistic approaches incorporating a divisive field in addition to the linear classic receptive field [Bonin et al., 2005]. The utility of using one model over another depends upon a variety of factors: the purpose of the experiment, the quality of the data and the size of the data being among the most important factors. However, are all these approaches equivalent? How should analysis performed using one method be understood using the other method? To understand this, I analyze these models for the features described in 3.1. I then discuss the conditions under which the fits from these models may be compared.

3.2.1 Classical Difference of Gaussian Receptive Fields

The classical Difference-of-gaussian receptive field model was explained in some detail in 2. I return to the model to understand its responses to the stimuli of various sizes.

Response of a Classical DOG Model to Arbitrary Patterns of Light

The receptive field is characterized by two independent gaussians ([Rodieck, 1965, Rodieck and Stone, 1965]):

$$RF\left(x,y\right) = K_c exp\left(\frac{-r^2}{r_c^2}\right) - K_s exp\left(^{-r^2}/_{r_s^2}\right) \tag{3.1}$$

$$r^2 = x^2 + y^2$$

$$x \subset \mathbb{R};\ y \subset \mathbb{R}$$

The contribution to the responses to a particular spot of light $\mathbb{I}$ at (x, y) equals $RF(x, y)\,\mathbb{I}\,dx\,dy$. The total response is the integral of the differential responses:

$$f\left(RF\left(x,y\right),\mathbb{I}\left(x,y\right)\right)=\int_{x}\int_{y}\left[K_{c}exp\left(^{-r^{2}}/_{r_{c}^{2}}\right)-K_{s}exp\left(^{-r^{2}}/_{r_{s}^{2}}\right)\right]\mathbb{I}\left(x,y\right)dx\,dy \quad (3.2)$$

Responses of the Classical DOG Model to Gratings Within an Expanding Aperture (Size Tuning)

One classic method to measure Size tuing in neurons involves measuring the response of neurons to gratings within an aperture of varying sizes. The tuning curve obtained is typically called Size-Tuning, or Area-Summation. What should area summation curves look like for a typical dLGN neuron in the rat? To model this, I consider a neuron with the following parameters:

$$r_c = 3^\circ;\; r_s = 12^\circ$$

$$K_c = 1;\; K_s = {}^{1}/_{16}(a.u.)$$

such that

$$\eta = 1$$

as defined in 2.2.9(see 2.2). The other critical parameter for performing this virtual experiment is the spatial frequency of the grating used to drive the neurons. For the purpose of this experiment, the spatial frequency used was the optimal spatial frequency obtained as in 2.1.

At the spatial frequency used, both the center and surround act as excitatory influences on the activity of the cell(Einevoll and Plesser 2005). The classic DOG model shows little suppression($\sim$ 2%) and displays peak response at $r_{Ap} \approx 15^\circ$. However, at higher spatial frequencies, the linear DOG model is capable of showing substantial suppression(3.3 and 3.4). The optimal summation radii were $r_{Ap} \approx 7.5^\circ$ (3.3a) and $r_{Ap} \approx 2.5^\circ$ (3.4b). Furthermore, responses showed substantial reduction: $\sim 21\%$ (3.3a) and $\sim 50\%$ (3.4b).

The center-surround receptive field and the spatial frequency of the grating used to drive the cell interact in complicated ways to result in the size tuning responses shown. In 3.2, until about $r_{Ap} = 5°$, the responses are driven primarily by the center subunit. However, beyond that the surround responses become significant. In this case, the spatial frequency is low enough that until $\sim 15°$, the center and surround have luminances of opposite sign: when the center has a light bar, the surround has a dark bar and vice-versa. The surround's influence is excitatory and the response increases further.

In 3.3, again we find that the center and surround act as excitatory influences on the response until $r_{Ap} = 10°$. However, the net increase in responses due to the surround is a smaller fraction of the increase due to the center (<30% in 3.3 compared to >50% in 3.2). At larger apertures, the surrounds integrates many cycles and its contribution is diminshed. At the largest apertures, the responses due to the classical surrounds are almost completely abolished.

In 3.4, however, the spatial frequency is high enough that the center itself is capable of integrating multiple cycles. We see that the peak response happens well before the center is reached. Beyond this radius, the center itself integrates multiple cycles leading to the first drop in response. At the largest apertures, most of the response has been abolished. This leads to high suppression($\sim 50\%$).

Contrast Dependence of Size Tuning with Classical DOG model

Does the DOG model show the features of real LGN neurons discussed earlier (see 3.1)? To test this, I simulate the responses of the linear DOG model to gratings of varying contrasts. The difference in the shape of the curve (compared to 3.2) is attributed to the log scale on the x-axis. It is unsurprising, that the response of the model neurons simply scales with contrast (3.5a,b). Contrast does not influence either suppression (3.5c) or the summation radius (3.5d).

Conclusions

In the above simulations, no attempt has been made to change the size and strength of the receptive field subunits across the different conditions of spatial

frequency and contrast. It might still be possible to recover the effects discussed in 3.1 with a linear Difference of Gaussian Receptive field whose Center and Surround kernels change with stimulus conditions. Such models have been proposed [Nolt et al., 2004, Sceniak et al., 2006, Sceniak et al., 2001] in the literature and will be taken up for further study in 3.2.3. However, in its current form, the simple Difference of Gaussians model while capable of explaining the presence of size tuning, is inherently incapable of explaining contrast saturation. A different model is required.

3.2.2 Divisive Normalization Models

Data indicating the inadequacy of the linear Difference of Gaussian receptive field in predicting LGN responses came from early work studying responses to different contrasts [Maffei and Fiorentini, 1973, Sclar et al., 1990]. It was further identified that suppressive phenomena exist in the dLGN through identifying effects that are independent of the sign of the luminance change but dependent on the size of the deviation [Levick et al., 1972]. This supported the idea of an Extraclassical Recepitve Field(ECRF) contributing to the responses of dLGN neurons. Stimulating the extraclassical receptive field never acted to drive the response of the neuron but were useful in suppressing the response of stimuli within the classical receptive field. Such extra-classical receptive fields were identified both in the retina [Victor, 1987] as well as in V1 [Carandini et al., 1997]. More recent theoretical work has identified a class of models capable of explaining many of these phenomena. First designed to explain contrast normalization within the retina [Victor, 1987], such models have been used to explain responses to contrast in the early visual system [Victor, 1987, Heeger, 1992, Freeman et al., 2002, Bonin et al., 2005]. We evaluate this model for the features described in 3.1.

Difference of Gaussian with Divisive Normalization

The schema for the Difference of Gaussian with Divisive normalization is provided in 3.6. Apart from the response of the linear center and surround kernels, an independent pathway calculates the standard deviation of the stimulus. This

is used to weight a spatially restricted suppressive field. The response of the suppressive field divides the response of the linear receptive field based on a half saturation contrast (c_{50}). The mathematical form of the model follows:

The Center and the surround linear kernels are denoted by

$$C_L(x,y) = K_c exp\left(-r^2/r_c^2\right) \tag{3.3}$$

and

$$S_L(x,y) = K_s exp\left(-r^2/r_s^2\right) \tag{3.4}$$

leading to the total linear kernel

$$RF_L(x,y) = K_c exp\left(-r^2/r_c^2\right) - K_s exp\left(-r^2/r_s^2\right) \tag{3.5}$$

$$r^2 = x^2 + y^2$$

$$x \subset \mathbb{R};\ y \subset \mathbb{R}$$

The non-linear surround weight is given by

$$S_E(x,y) = K_E exp\left(-r^2/r_E^2\right) \tag{3.6}$$

$$x \subset \mathbb{R};\ y \subset \mathbb{R}$$

along with the half saturation contrast, c_{50}. For a given pattern of light $\mathbb{I}(x,y)$, the linear response of the cell is given by

$$f_L\left(RF_L(x,y), \mathbb{I}(x,y)\right) = \int_x \int_y \left[K_c exp\left(-r^2/r_c^2\right) - K_s exp\left(-r^2/r_s^2\right)\right] \mathbb{I}(x,y)\, dx\, dy \tag{3.7}$$

The non-linear local contrast c_{local} is calculated by weighting the squared stim by the non-linear surround weight:

$$c_{local}\left(S_E\left(x,y\right),\mathbb{I}\left(x,y\right)\right)=\sqrt{\int_x\int_y\left[K_E exp\left(^{-r^2}/_{r_E^2}\right)\right]\mathbb{I}^2\left(x,y\right)dx\,dy} \tag{3.8}$$

Note the squaring term on the image luminance. This prevents any pattern of light $I(x,y)$ from ever contributing negatively to the local contrast c_{local}. The lowest possible value of c_{local} is zero and this happens when the overall luminance on the screen is the mean luminance (=0). All other patterns contribute positively. Finally, the net response of the cell is

$$f(RF_L,S_E,I)=f_L*\frac{c_{50}}{c_{50}+c_{local}} \tag{3.9}$$

Size tuning with Divisive Normalization

The response of the non-linear surround is positive and increases with both the Michelson Contrast (defined as $\left(\frac{\mathbb{I}_{max}-\mathbb{I}_{min}}{\mathbb{I}_{max}+\mathbb{I}_{min}}\right)$ for any pattern of light $\mathbb{I}(x,y)$) of the stimulus as well as the size of the stimulus. Thus this model treats both these factors identically and one would expect the responses at large aperture sizes to be lower than the responses at small aperture sizes. Thus even conditions that did not show substantial suppression (like in 3.2) start showing suppression.

The neuron modeled in 3.7a is identical to the one in 3.5 with a normalizing suppressive field. The comparison shows how the suppresive field can show divisive normalization. As the size of the stimulus increases, the overall contribution of the suppressive field increases. This increase is independent of the sign of the luminance because of the presence of the squaring non-linearity. Even though the linear receptive field's contribution is still increasing, the contribution due to the non-linear surround overwhelms that due to the classical receptive field leading to strong suppression and clear size tuning.

Contrast saturation with Divisive Normalization

As seen in 3.7b, the response of the single unit at large apertures; a proxy for full-field contrast response of the unit shows clear saturation (red crosses).

The linear component (black crosses) itself shows no saturation. The saturating responses are well fit by a hyperbolic function (red curve), while the non-saturating responses are well fit by a straight line.

Contrast Dependent Suppression and Summation Radius

As seen in 3.7c and d, the amount of suppression as well as optimal summation radius (r_{opt}) is dependent on the michelson contrast of the stimulus. To understand the reason for this, lets qualitatively estimate the non-linear surround contribution both at the peak response aperture and at full-field aperture for two different michelson contrasts. At low enough michelson contrasts, c_{local} is small at all aperture sizes. The non-linear contribution tends to 1. The suppression seen is from the linear receptive field, a value estimated to be small as shown in 3.2.1. At higher michelson contrasts, the contribution of the non-linear surround goes from negligible ($\ll c_{50}$) to dominating ($\gg c_{50}$). This explains why the overall suppression is different at different contrasts: higher contrasts show higher suppression.

This further expains how the optimal summation radius (r_{opt}) increases at lower contrasts. Compared to low contrast responses, the increase in the non-linear contribution at higher michelson contrast as well as with aperture radius cause the size tuning to peak earlier.

Conclusions

It is clear that divisive normalization can explain all the features discussed in 3.1. In additions to these features, it can further address other kind of responses like masking [Bonin et al., 2005, Solomon et al., 2002]. Fitting dLGN responses with divisive normalization may provide models with the greatest predictive power. Once the model is fit, the parameters involved do not change and can then be used to predict responses for more complex stimuli. However, fitting these models require large amounts of data; data that is usually hard to obtain in awake preparations.

3.2.3 Modified DOG Receptive Fields

Other approaches to fitting area tuning curves have been attempted. These approaches typically involve relaxing the assumption of constant linear center and surround receptive field properties across stimuus conditions. While it has the advantage of not requiring large quantities of data to fit the model, it has the disadvantage of being phenomenological. I discuss two models that are likely to show more of the response properties detailed in 3.1.

Contrast Dependent Change in Surround Strength

As discussed in 3.2.1, the classical center and surround can both contribute to suppression of responses. However, with constant center and surround strength and sizes, it was impossible to see contrast dependent size tuning, full field contrast saturation or optimal summation radius (3.5).

However, what would happen is we can change the strength of the classical surround?

3.8 shows the responses of a model neuron where the strength of the surround K_s is dependent on the michelson contrast of the stimulus. In this model, surround strength increases linearly with contrast. This model allows for contrast dependent suppression but does not allow contrast saturation or for a contrast dependent optimal summation radius.

Conclusion

While the DOG model itself is not capable of explaining many of the response properties of real neurons, relaxing assumptions about the size and strength of the receptive fields can yield better fits to responses of real neurons. It would be instructive to attempt changing the parameters systematically to find those changes which best fit the responses of real neurons.

Chapter 3, in part, is being prepared for submission for publication of material. Sriram, Balaji; Reinagel, Pamela. The dissertation author was the primary investigator and the first author of the paper.

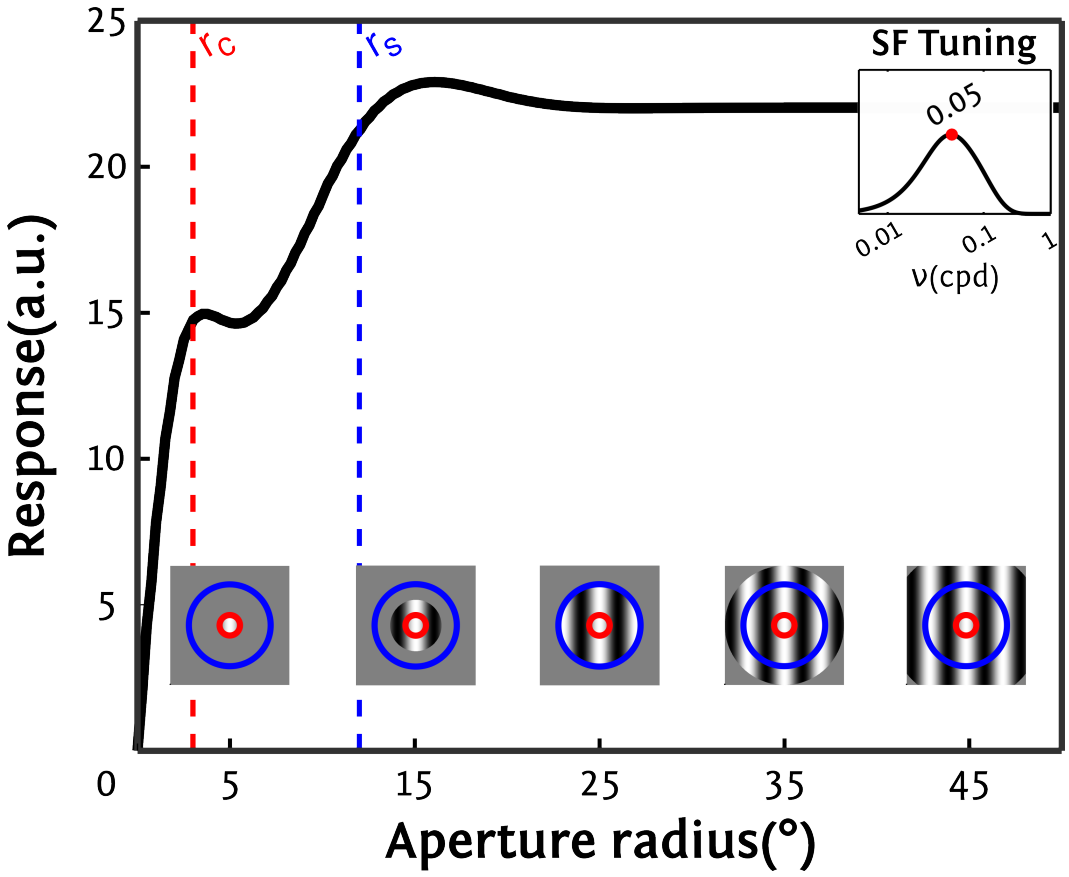

Figure 3.2: **Size Tuning Curve for a model neuron.**
The model neuron here has $r_c = 3°$ and $r_s = 12°$ with a balanced classical surround (see 2.3.2 for definitions). The response of the model cell is dependent on the size of the aperture. Bottom insets show the extent of the center and surround as well as the aperture of the stimulus used to drive the neuron. The red and blue circles indicate the 2SD of the center and surround gaussian densities and the stimulus within circular apertures is overlaid on top. Top inset shows the spatial frequency tuning as estimated from 2.1. The spatial frequency used for the size-tuning experiment is denoted as a red dot on the spatial frequency tuning curve; the exact value of the spatial frequency (in *cpd*) is also included.

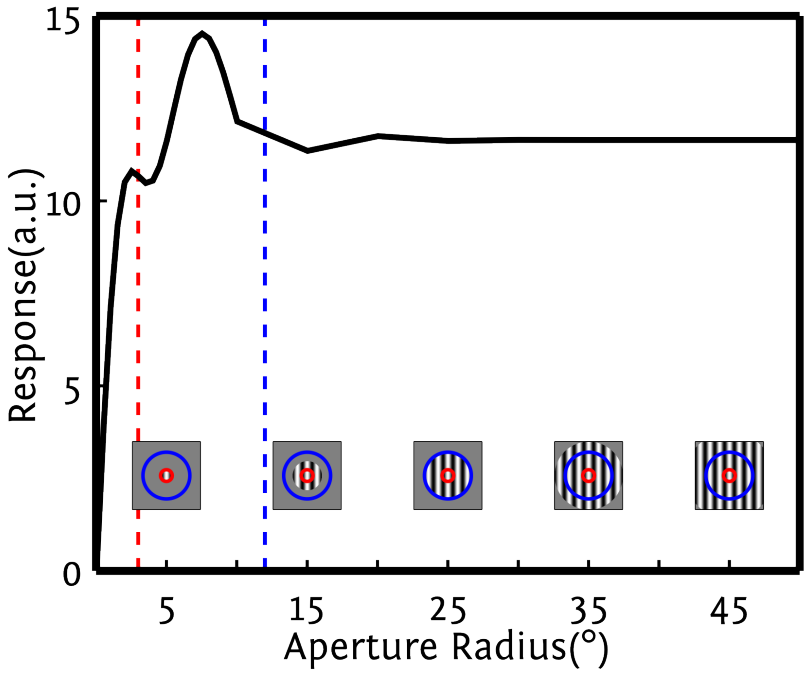

Figure 3.3: **Responses show higher suppression at high spatial frequency.** The model neuron shown here has $r_c = 3°$ and $r_s = 12°$ with a balanced classical surround (as in 3.2). The spatial frequency of the grating used to drive the cell was $\nu = 0.1$ *cpd*. Bottom insets show the extent of the center and surround (as explained in 3.2) as well as the aperture of the stimulus used to drive the neuron.

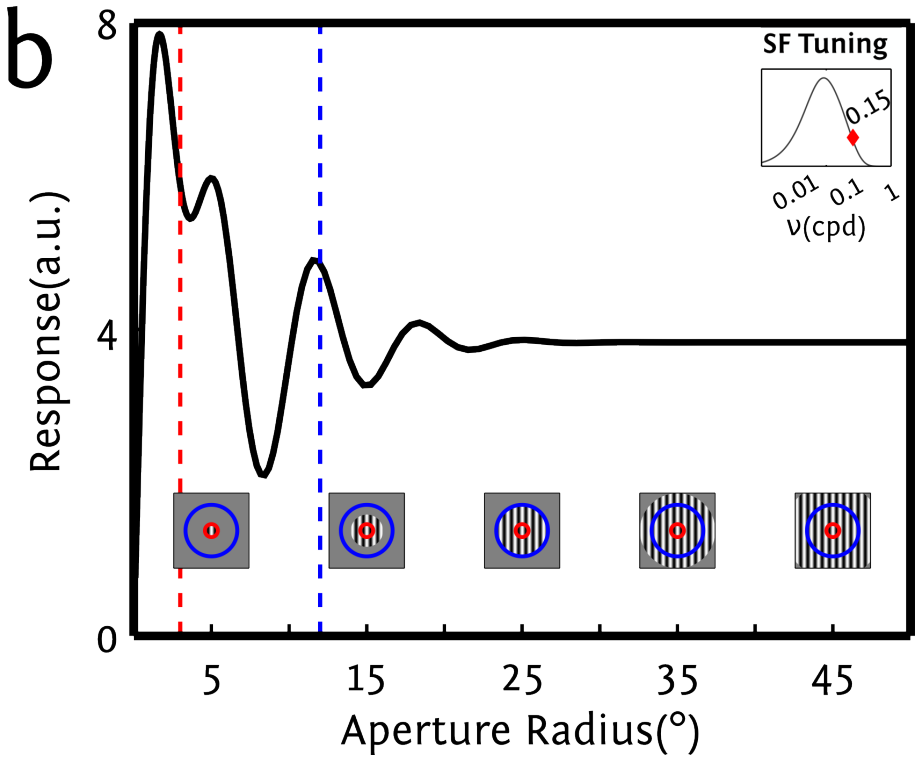

Figure 3.4: **Responses show suppression at high spatial frequencies.** The model neurons shown here has $r_c = 3°$ and $r_s = 12°$ with a balanced classical surround (as in 3.2). The spatial frequency of the grating used to drive the cell was $\nu = 0.15$ *cpd*. Top insets show the spatial frequency tuning of the neuron. The spatial frequency used to drive the cell is denoted by a red dot; the value of the spatial frequency is also noted (in *cpd*). Bottom insets show the extent of the center and surround (as explained in 3.2) as well as the aperture of the stimulus used to drive the neuron.

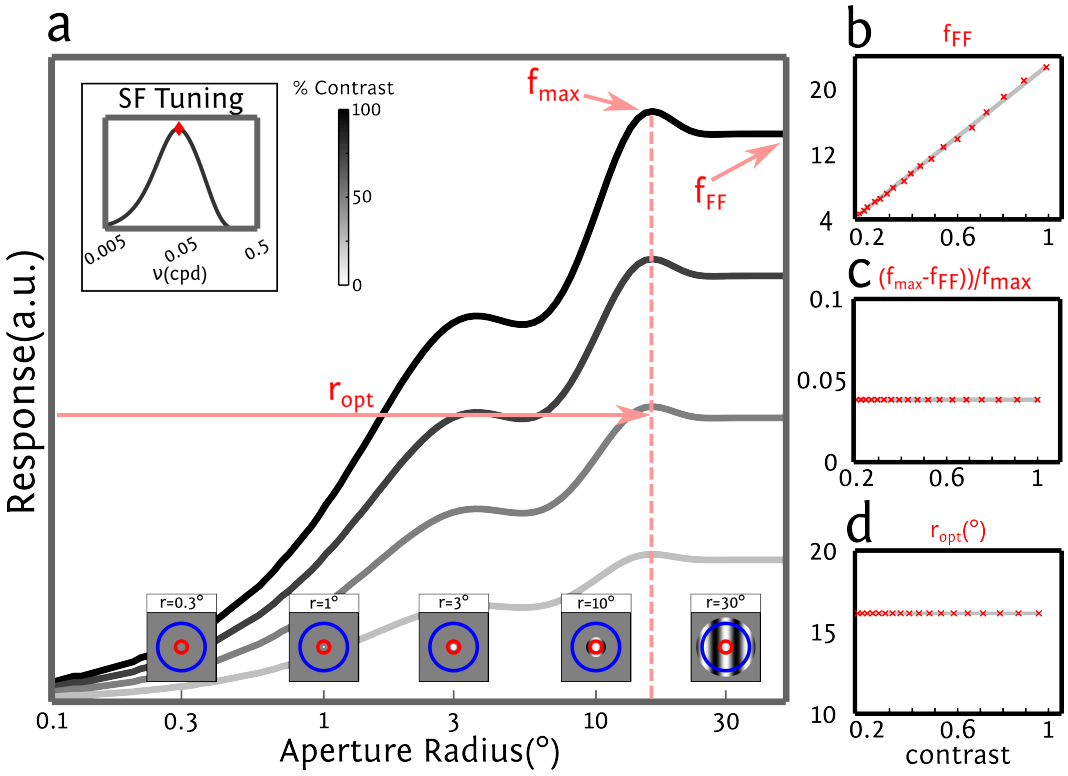

Figure 3.5: **Contrast Dependence of Size Tuning to Linear DOG Model.** **a** shows the size-tuning response of the neuron described in 3.2 to gratings of varying contrasts. Top insets show the spatial frequency tuning as well as the contrast color scale used to plot the size-tuning curves.Bottom insets show the stimulus context at various aperture radii. It defines the maximal response f_{max}, the response at full field f_{FF}, and the optimal radius (radius at maximal response) r_{opt}. **b** shows the contrast response curve (fullfield response f_{FF}) as a function of contrast. Red crosses indicate the model response and the grey curve is best fit line to the contrast response curve. **c** shows the suppression $\frac{f_{max}-f_{FF}}{f_{max}}$ as a function of contrast while **d** shows the optimal radius (r_{opt}) as a function of contrast.

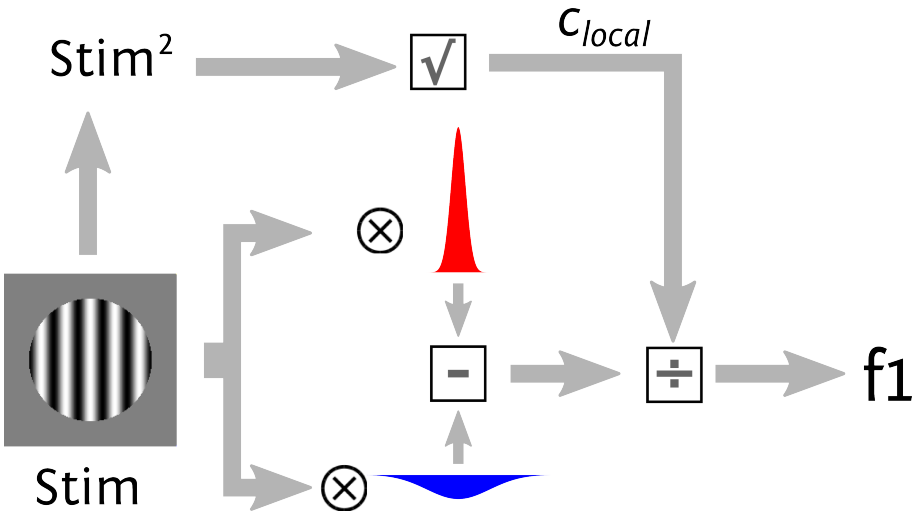

Figure 3.6: **DOG with Divisive Normalization.**
Any stimulus passes through two independent paths. the first path is the DOG model explained in 3.2.1. The response calculated by the linear receptive field is normalized by an independent pathway that calculates the local contrast, c_{local}. This suppressive pathway calculates the local contrast as the standard deviation of the stimulus. The net response $f1$ is the ratio of the linear response and the divisive field response.

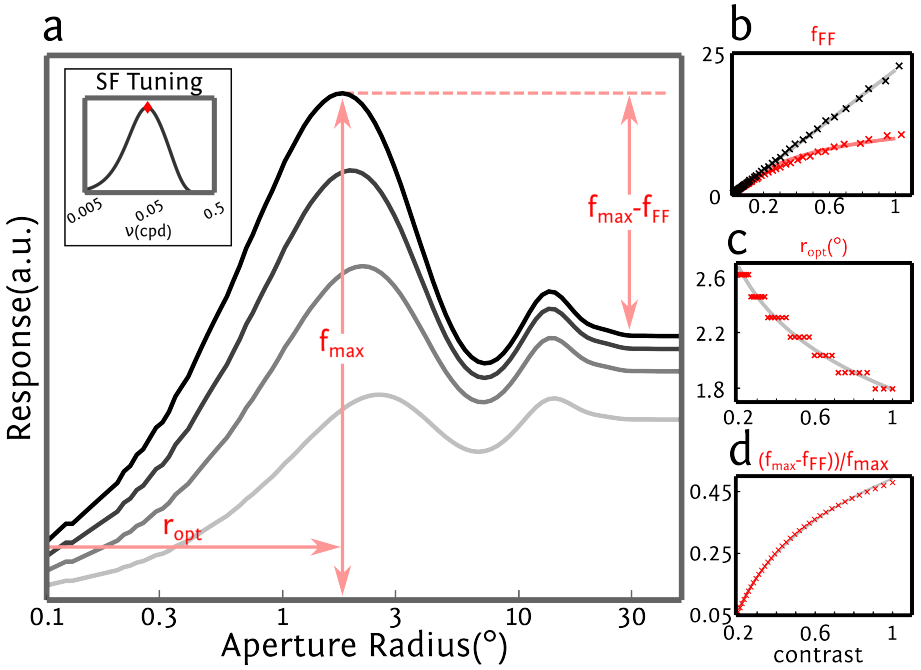

Figure 3.7: **Size Tuning for DOG with Divisive Normalization.** **a** The response of the receptive field explained in 3.2 and in 3.5 with a non-classical surround added. Non classical surround parameter values are: $r_E = 16$, $K_E = 30$ and $c_{50} = 0.1$. **b** The values of the responses at the maximum aperture is used as a proxy for full field response (f_{FF}). The contrast response curve of the cell with divisive normalization shows saturation. The red line is the best hyperbolic fit (of the form $f(c) = \dfrac{f_{max}c}{c_{50}+c}$) to the data. The linear receptive field's response alone (black crosses) does not show saturation. the light grey curve is the best fit line to the linear receptive field response. **c** The optimal response radius r_{opt} decreases with an increase in contrast. Estimated optimal radii (red crosses) are well fit by a decaying exponential curve. **d** The overall suppression is contrast dependent. Suppression calculated as $supp = \dfrac{f_{max} - f_{FF}}{f_{max}}$ increases with an increase in contrast. The estimated suppression (red crosses) is well fit by an increasing exponential.

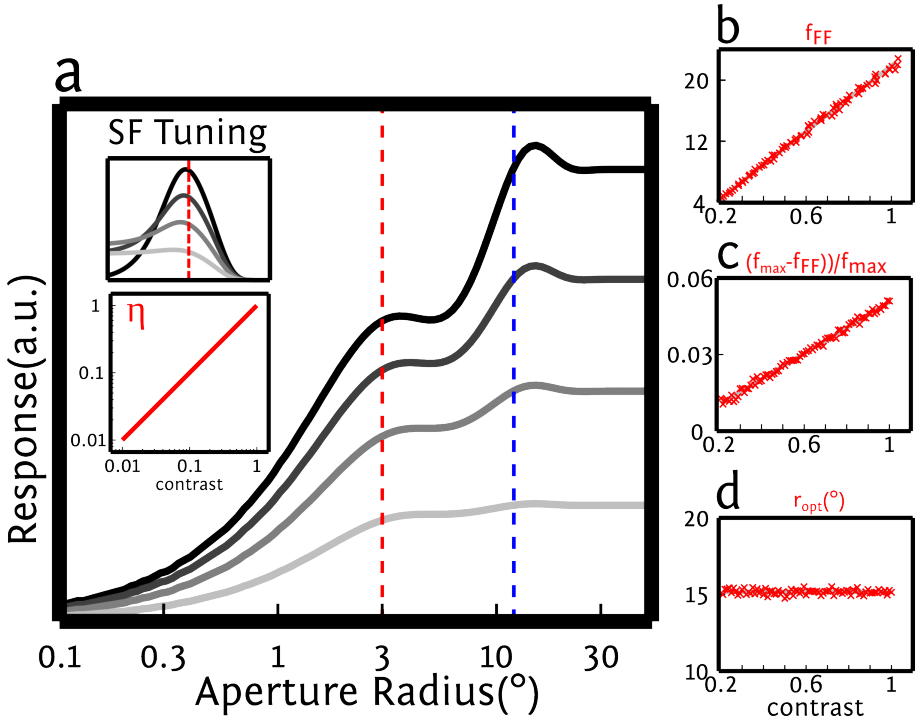

Figure 3.8: **Size Tuning for DOG with Variable Surround Strength.** **a** Size tuning for a classical DOG model with variable surround strength. Top inset shows the spatial frequency tuning of the neuron at different contrasts. Dotted red line indicates the spatial frequency used to simulate the size tuning curve. Bottom inset shows the strength of the surround as a function of the michelson contrast. **b**The values of the responses at the maximum aperture is used as a proxy for full field response (f_{FF}). The contrast response curve does not show saturation. **c** The overall suppression is contrast dependent. Suppression calculated as $supp = \frac{f_{max} - f_{FF}}{f_{max}}$ increases with an increase in contrast. The estimated suppression (red crosses) is well fit by an straight line. **d** The optimal response radius r_{opt} does not change with contrast.

Chapter 4

Size Tuning in the Rodent dLGN

4.1 Introduction

Responses of the neurons in the dLGN are shaped by powerful linear and non-linear influences. What contributes to these influences? Atleast in part, dLGN responses are inherited from its input, the retina. Physiological and anatomical evidence suggests that, in the cat, X-cells receive very few retinal inputs and that typically a single input dominates the responses of the geniculate neuron [Levick et al., 1972, LeVay and Ferster, 1979]. However, the local circuitry in the dLGN plays a large role in shaping their responses [Lindstrom and Wrobel, 2011, Butts et al., 2011, Wilson et al., 1996, Wang et al., 2007]. Apart from the immediate circuitry, dLGN responses are affected by the state of the animal: sleep [Livingstone and Hubel, 1981], anesthesia [Pape and Eysel, 1988], attention [McAlonan et al., 2008] and via the massive feedback from cortex [Olsen et al., 2012, Sillito et al., 2006, Andolina et al., 2007]. It is, however, still a matter of debate as to the exact cause of the responses of dLGN neurons. Recent years has seen the use of rodents in studying the circuitry causing these responses. The ability to genetically target a specific subpopulation of neurons has allowed for precise manipulation of their activity leading to a more detailed understanding of the circuitry involved. However, to understand the role that specific neuronal sub-types may be playing in the responses described in 3.1, we will need to test the presence of these features in the rodent preparation.

To test for the presence of the responses described in 3.1, I recorded size tuning curves in awake rodents. Multiple reasons prevent me from performing the kind of analyses explained in 3:

- **Limitation in recording times:** As explained in 3.2.2, large quantities of data is required to model the complete model (see 3.9). One needs to locate the center of the receptive field, measure the spatial frequency tuning of the neuron, obtain contrast tuning of neurons, and finally obtain the size tuning graphs at multiple different contrasts. Initial characterization typically take from 10 to 15 minutes in the awake preparation. This is the median length of any recorded neuron. Improvements in the recording technique will enable us to increase recording lengths in the future allowing us to get higher quantities of data.

- **Eye movements:** The presence of eye movements will affect the centering of the stimulus over the receptive field. As explained in 2.2.6, eye movements were small and infrequent. However, since many of the features we wish record happen on the scale of the receptive field center of dLGN neurons, even small eye movements would affect the measurements. With long recording times, it may be possible to average over these effects. However, such long recordings are hard in awake rodents.

- **Unexpected responses:** Some neurons show responses not expected by any of the models explained in 3.

In view of the above reasons, I present the recorded data as is. I detail the parameters of the recording and mention the examples which do not conform to our expectations of such responses.

4.2 Methods

The method for recording single units in the awake rodent dLGN is identical to that mentioned in 2.2. However, a few more details are provided for completion.

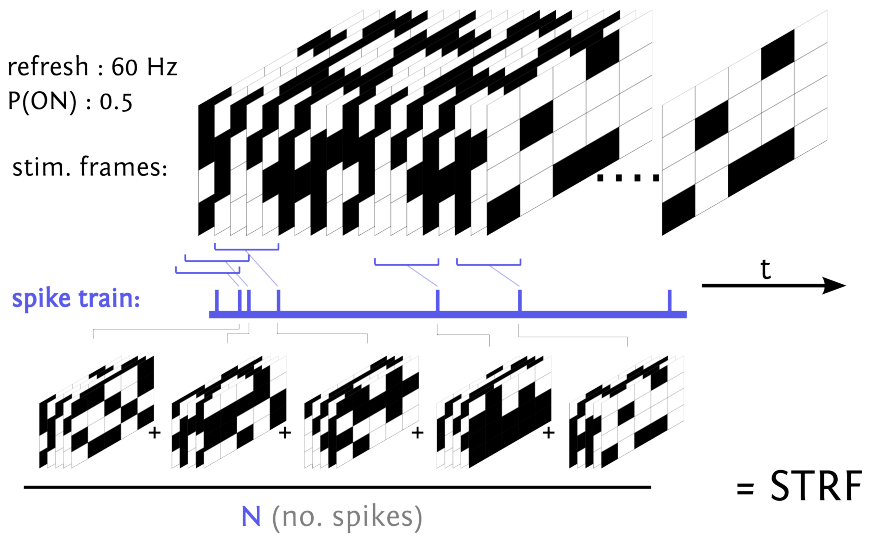

Figure 4.1: **Identifying Spatio-Temporal Receptive Fields.**
The screen was split into 5° or 2.5° squares. On each frame, each square was either completely ON or OFF. The choice of whether it was completely ON or OFF was made pseudo-randomly with a probability $P_{ON} = 0.5$. This pseudo-random stimulus was repeated 60 times a second. Simultaneously, spike trains from dLGN neurons are recorded. The average stimulus that preceded the spike was then used to calculate the average spatio-temporal receptive field (STRF/STA).

4.2.1 Locating the Receptive Field Center

Receptive fields were located with white noise stimuli [Chichilnisky, 2001]. Briefly, a random checkerboard stimulus was presented on the monitor for each frame; the frame rate of the monitor was 60 Hz. Simultaneously recorded single units were used to used to calculate the average stimulus preceding a spike: the spatio temporal receptive field (STRF) or the spike triggered average (STA) (see 4.1 for a schema).

The calculated STA provides the shape of the receptive field over time. As shown in 4.2, the center of the receptive field integrates stimuli faster and shows an earlier peak sensitivity (83 ms). A 2-D gaussian was fit to the spatial STA at the time of maximal sensitivity. The center of the gaussian was the estimated center of the receptive field.

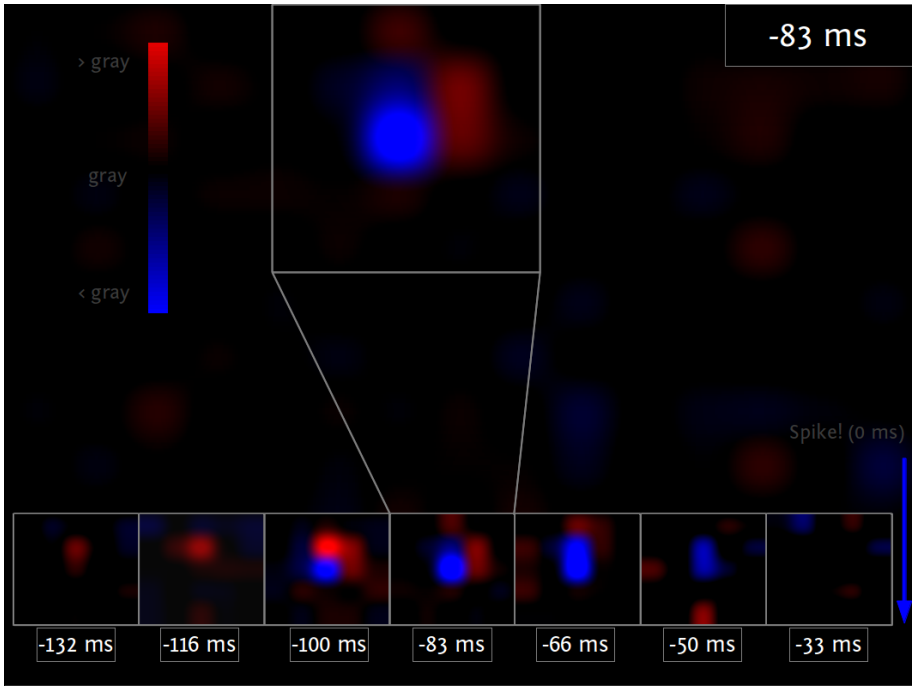

Figure 4.2: **Example Spatio-Temporal Receptive Field**
Example STRF of an OFF center cell. Bottom insets shows the spike triggered average over time. Time preceding the spike increases to the left. The average stimulus preceding each spike is a gray screen 33ms before the spike. The average stimulus was below gray screen 50 ms and is the lowest 83 ms prior to the spike. The center of the receptive field is not influenced by stimuli more than 100 ms before the spike. The surround is slower. Its influence starts later then the center's infleunce (66 ms) and peaks later (100 ms). The figure shows the overall STRF across the entire screen 83 ms before the spike.

4.2.2 Choosing Spatial Frequency

Independent of the actual spatial frequency preference of the LGN neurons, the spatial frequency used was $\nu = 0.1\,cpd$ or $\nu = 0.2\,cpd$.

4.2.3 Effect of Eye Movements

Eye movements were measured using an IR-eye tracking camera. Preliminary experiments indicated that eye movements were small (typically $< 5°$), rare ($< 1Hz$) and unrelated to the stimulus when stimulus speed was fast enough. For slower stimuli, the eyes locked to the leading edge of a grating exhibiting the

Opto-kinetic reflex. Such eye movements were small enough to measure spatial frequency tuning. However, measuring size tuning requires far more precise control over the gaze of the animal - a level of control not available in the awake rodent. The effects of eye movements will affect size tuning measurements the greatest for small apertures. Spike modulation amplitudes for aperture sizes below 10° are likely to be inaccurate. Considering that the greatest influence on the size of the response is due to the center, eye movements will tend to suppress the responses of neurons. Hence, responses at small aperture radii are likely to be underestimates of their true value.

4.3 Results

The individual size-tuning curves follow. For each single unit, I include analyses of the receptive field location, as well as the measured size-tuning curve at various contrasts. If multiple contrasts have been used, the value of the contrasts is also mentioned.

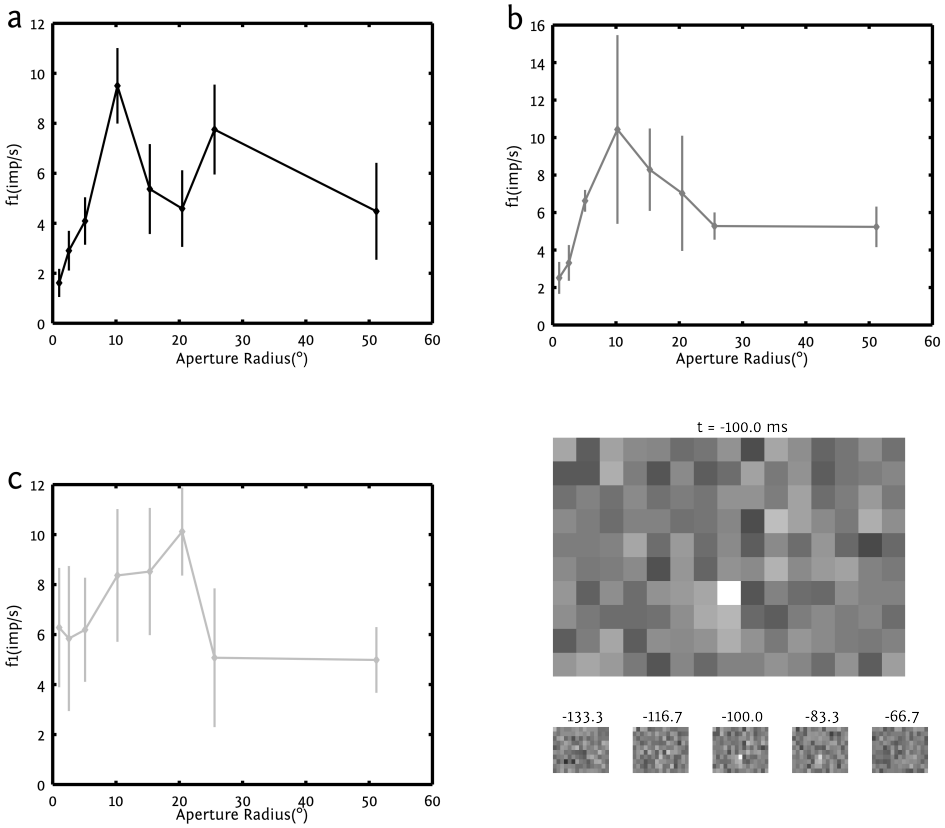

Figure 4.3: **Size Tuning for Neuron ID:3**
The Figure shows size Tuning for Neuron #3. X-Axis is the aperture size in degrees while y-axis is amplitude of the modulation in impulses/s. The nominal contrast used was 1 (in **a**) 0.5 (in **b**) and 0.25 (in **c**). Also included is the spatio-temporal receptive field (bottom right). Large panel shows the spatial context at the maximal deviation of the STA (t = 100 ms prior to spike). Each square is 5° in size. Small insets below show the spatial context before, during and after the context in the large panel.
Responses do not reduce with contrast.

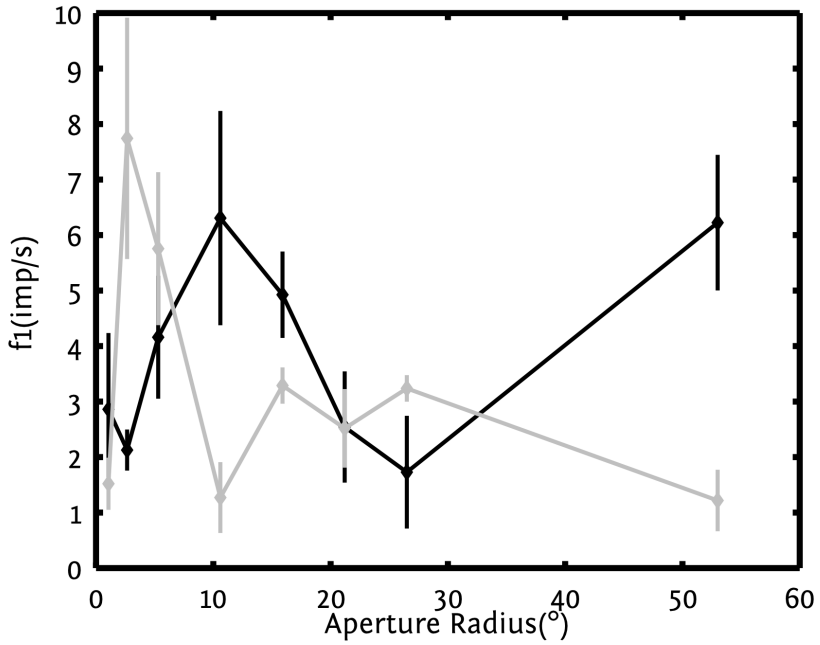

Figure 4.4: **Size Tuning for Neuron ID:7**
The Figure shows size Tuning for Neuron #7. X-Axis is the aperture size in degrees while y-axis is amplitude of the modulation in impulses/s. The nominal contrast used was 1 (dark curve) and 0.25 (light gray curve).

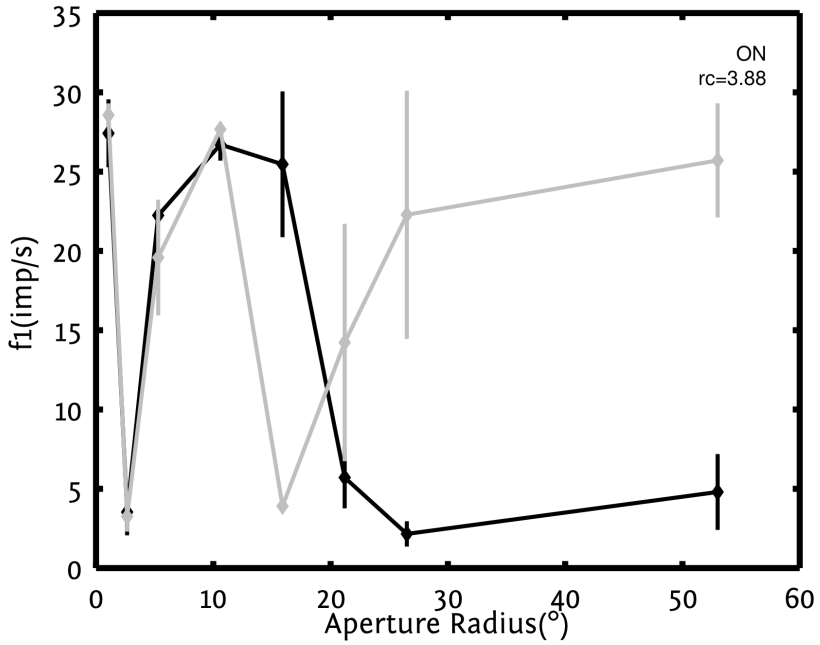

Figure 4.5: **Size Tuning for Neuron ID:9**
The Figure shows size Tuning for Neuron #9. X-Axis is the aperture size in degrees while y-axis is amplitude of the modulation in impulses/s. The nominal contrast used was 1 (dark curve) and 0.25 (light gray curve).

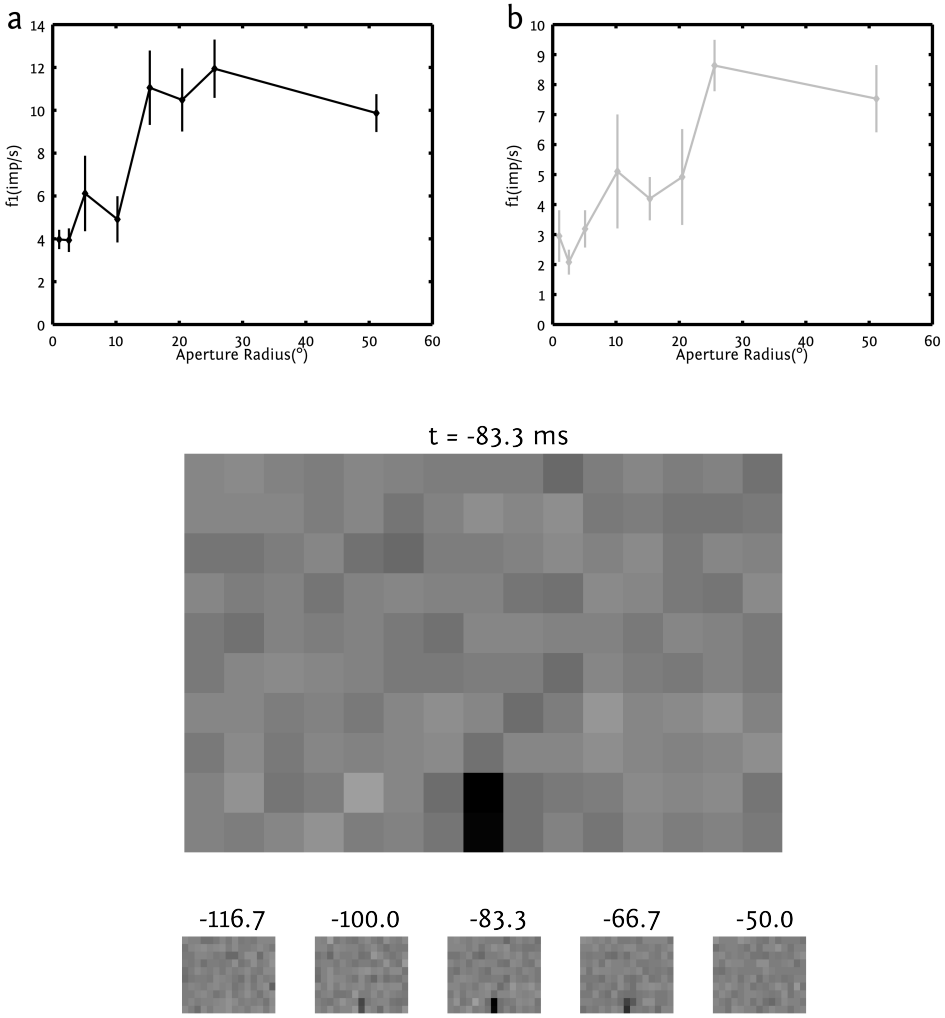

Figure 4.6: **Size Tuning for Neuron ID:12**
The Figure shows size Tuning for Neuron #12. X-Axis is the aperture size in degrees while y-axis is amplitude of the modulation in impulses/s. The nominal contrast used was 1 (in **a**) and 0.25 (in **b**). Also included is the spatio-temporal receptive field (bottom). Large panel shows the spatial context at the maximal deviation of the STA (t = 83 ms prior to spike). Each square is 5° in size. Small insets below show the spatial context before, during and after the context in the large panel.

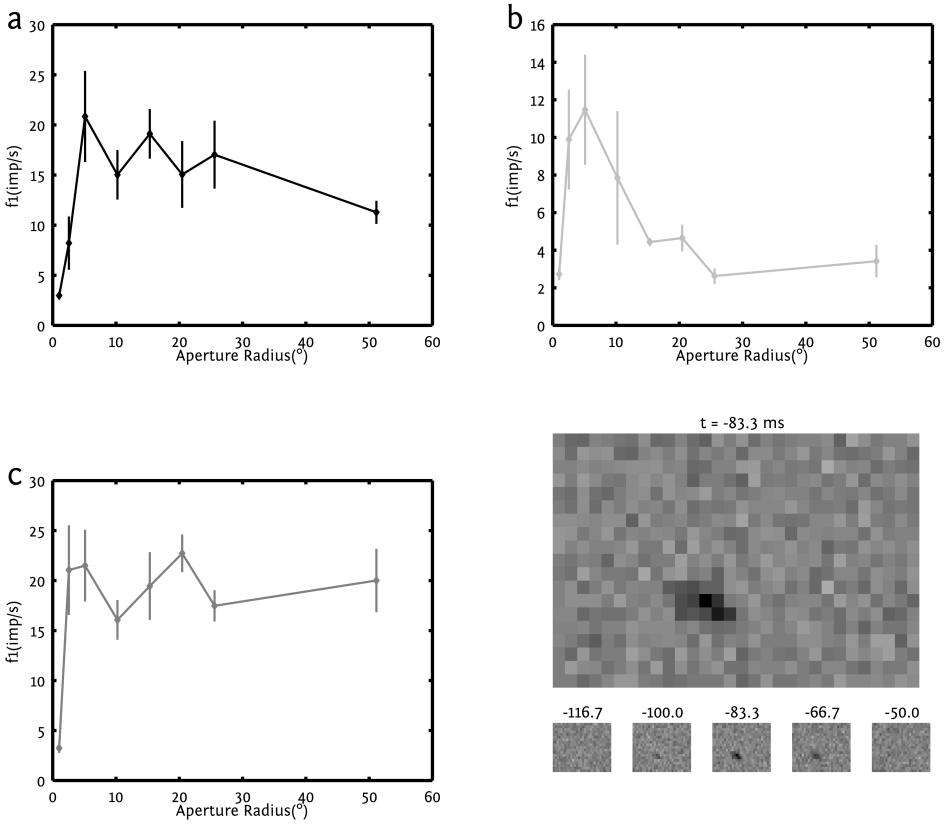

Figure 4.7: **Size Tuning for Neuron ID:14**
The Figure shows size Tuning for Neuron #14. X-Axis is the aperture size in degrees while y-axis is amplitude of the modulation in impulses/s. The nominal contrast used was 1 (in **a**) 0.25 (in **b**) and 0.5 (in **c**). Also included is the spatio-temporal receptive field (bottom). Large panel shows the spatial context at the maximal deviation of the STA (t = 83 ms prior to spike). Each square is 2.5° in size. Small insets below show the spatial context before, during and after the context in the large panel.

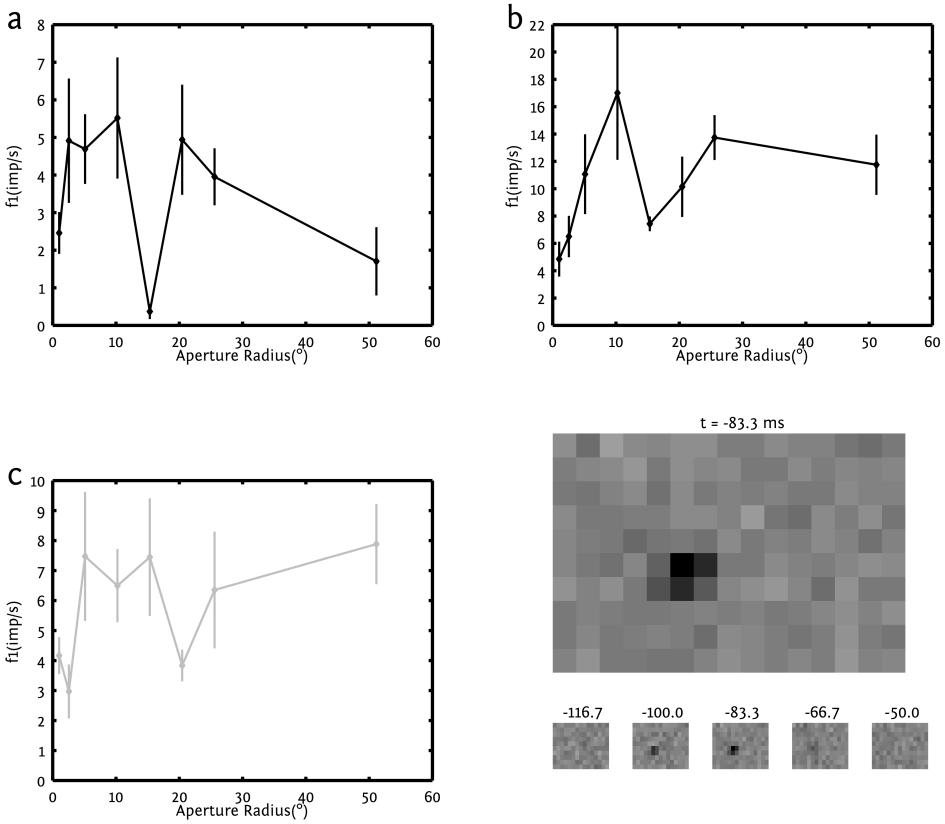

Figure 4.8: **Size Tuning for Neuron ID:16**
The Figure shows size Tuning for Neuron #16. X-Axis is the aperture size in degrees while y-axis is amplitude of the modulation in impulses/s. The nominal contrast used was 1 (in **a** and **b**), 0.25 (in **c**) and 0.5 (in **d**). Also included is the spatio-temporal receptive field (bottom). Large panel shows the spatial context at the maximal deviation of the STA (t = 83 ms prior to spike). Each square is 5° in size. Small insets below show the spatial context before, during and after the context in the large panel.

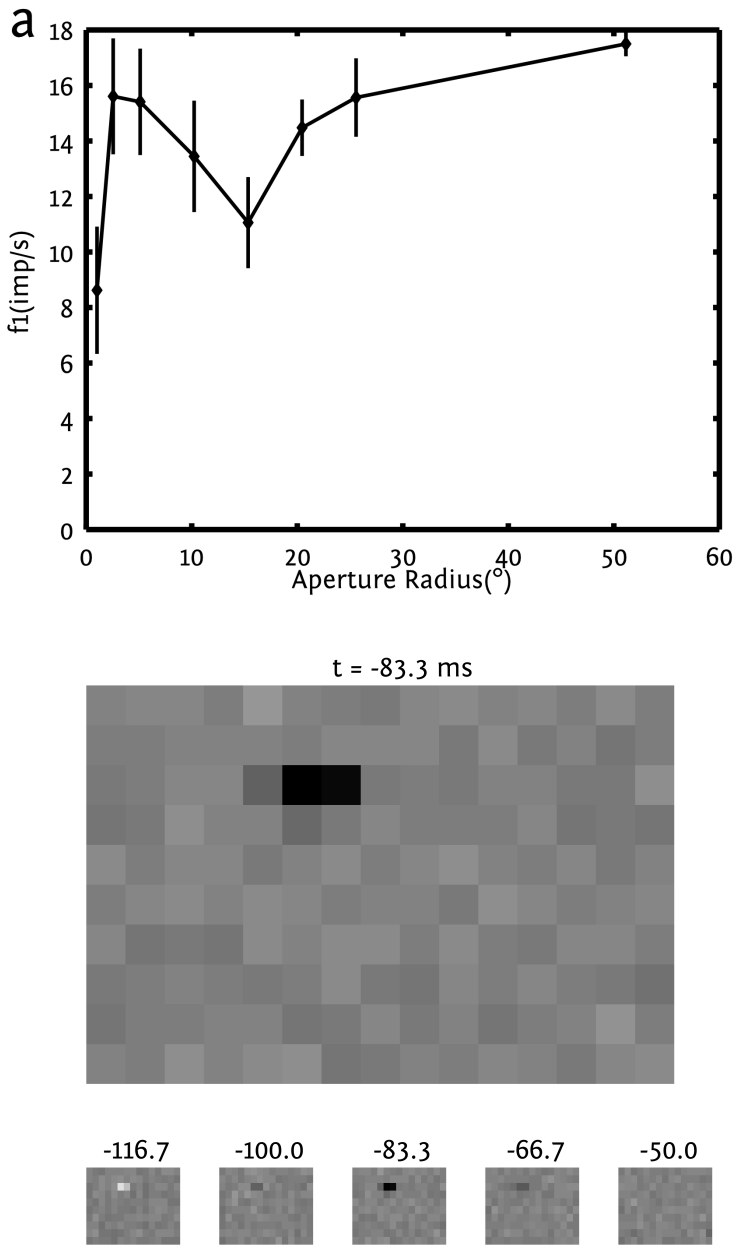

Figure 4.9: **Size Tuning for Neuron ID:17**
The Figure shows size Tuning for Neuron #17. **a** X-Axis is the aperture size in degrees while y-axis is amplitude of the modulation in impulses/s. The nominal contrast used was 1. Also included is the spatio-temporal receptive field (right). Large panel shows the spatial context at the maximal deviation of the STA (t = 83 ms prior to spike). Each square is 5° in size. Small insets below show the spatial context before, during and after the context in the large panel.

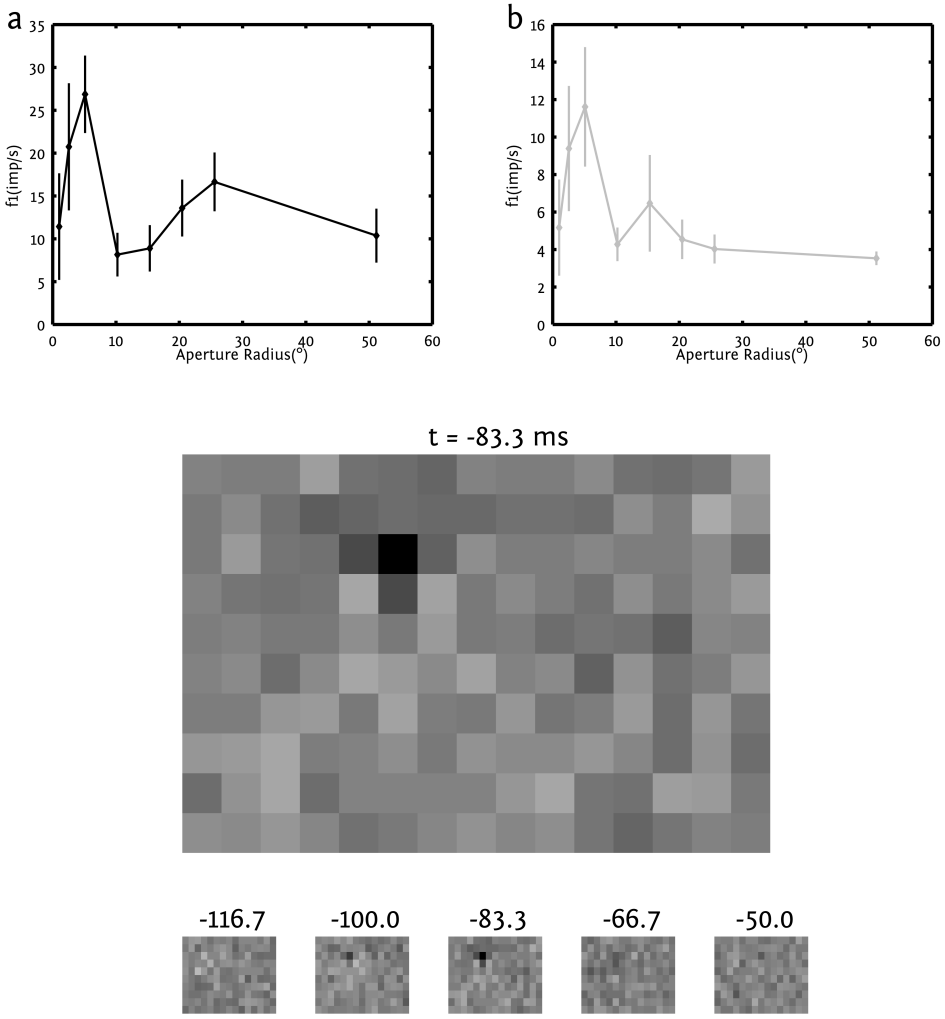

Figure 4.10: **Size Tuning for Neuron ID:22**
The Figure shows size Tuning for Neuron #22. **a** X-Axis is the aperture size in degrees while y-axis is amplitude of the modulation in impulses/s. The nominal contrast used was 1. Also included is the spatio-temporal receptive field (right). Large panel shows the spatial context at the maximal deviation of the STA (t = 83 ms prior to spike). Each square is 5° in size. Small insets below show the spatial context before, during and after the context in the large panel.

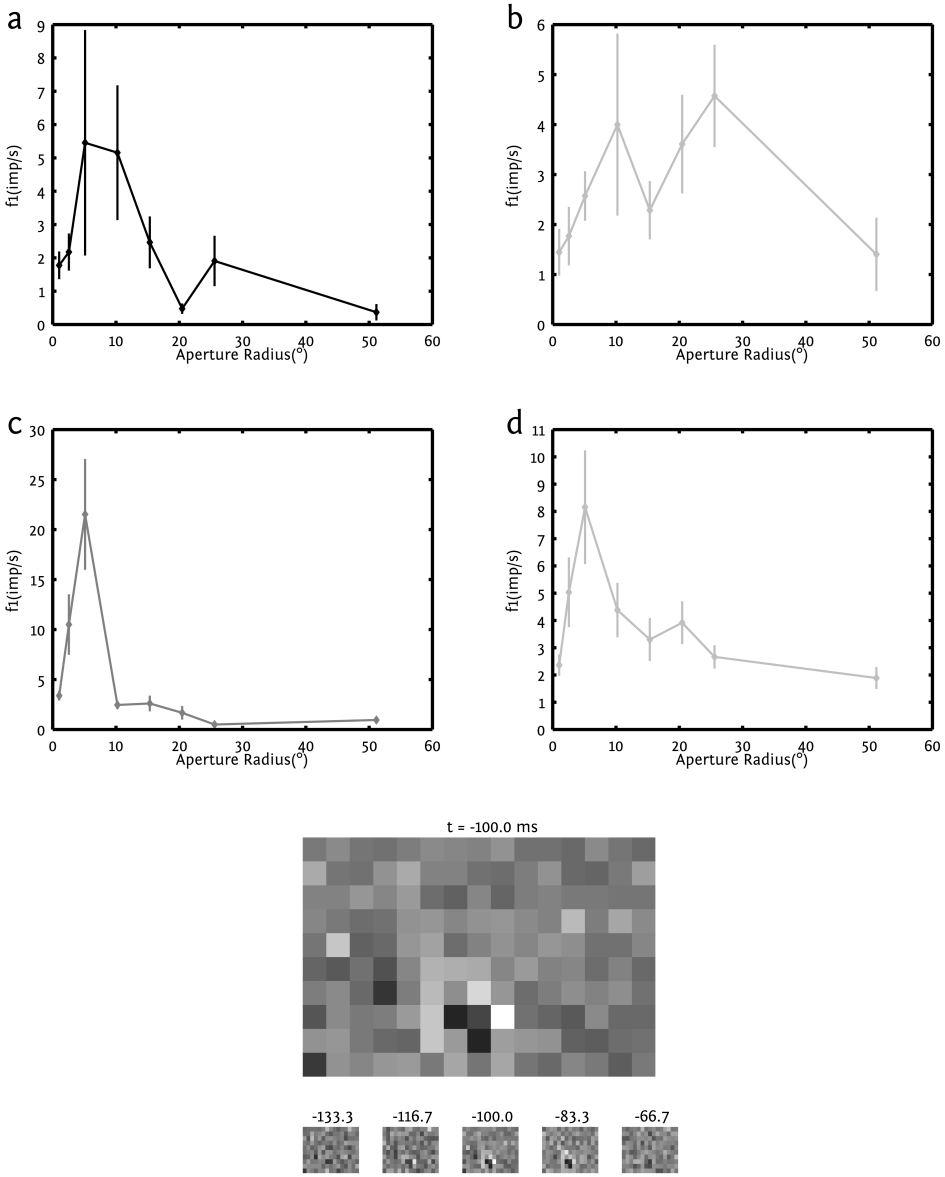

Figure 4.11: **Size Tuning for Neuron ID:26**
The Figure shows size Tuning for Neuron #26. X-Axis is the aperture size in degrees while y-axis is amplitude of the modulation in impulses/s. The nominal contrast used was 1 (in **a**), 0.25 (in **b**), 0.5 (in **c**) and 0.25 (in **d**). Also included is the spatio-temporal receptive field (bottom). Large panel shows the spatial context at the maximal deviation of the STA (t = 100 ms prior to spike). Each square is 5° in size. Small insets below show the spatial context before, during and after the context in the large panel.

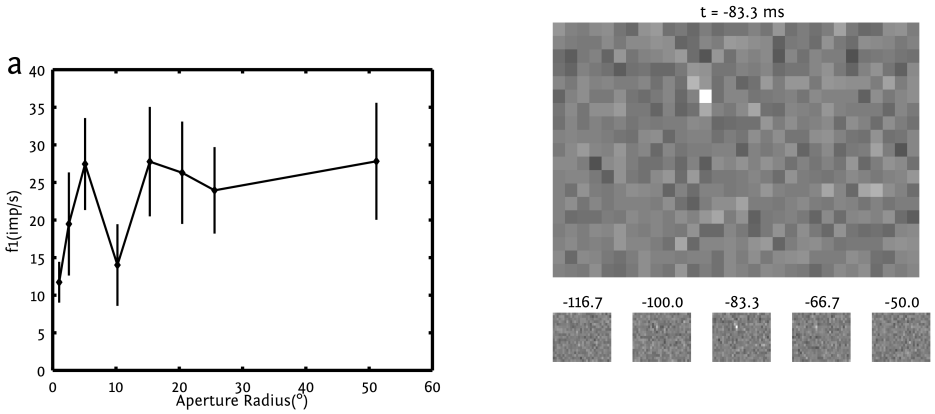

Figure 4.12: **Size Tuning for Neuron ID:33**
The Figure shows size Tuning for Neuron #33. **a** X-Axis is the aperture size in degrees while y-axis is amplitude of the modulation in impulses/s. The nominal contrast used was 1. Also included is the spatio-temporal receptive field (right). Large panel shows the spatial context at the maximal deviation of the STA (t = 83 ms prior to spike). Each square is 2.5° in size. Small insets below show the spatial context before, during and after the context in the large panel.

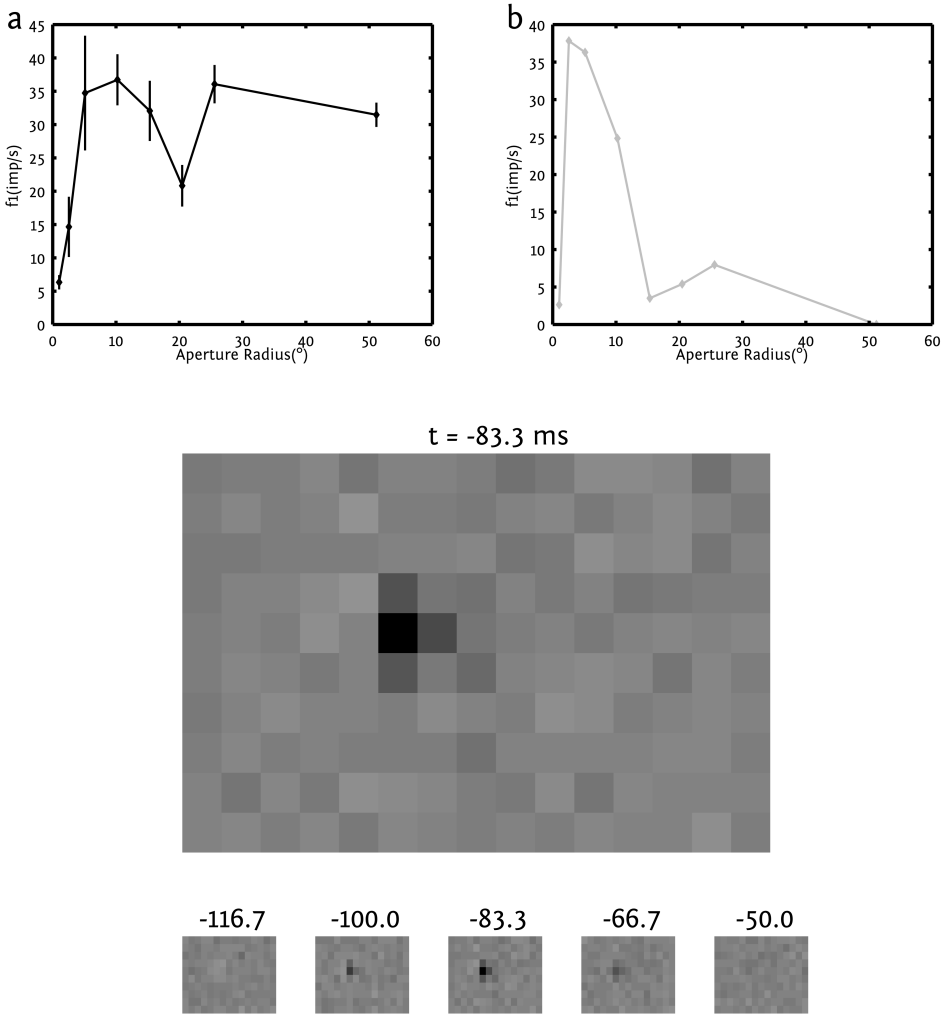

Figure 4.13: **Size Tuning for Neuron ID:37**
The Figure shows size Tuning for Neuron #37. **a** X-Axis is the aperture size in degrees while y-axis is amplitude of the modulation in impulses/s. The nominal contrast used was 1 (in **a**) and 0.25 (in **b**). Also included is the spatio-temporal receptive field (bottom). Large panel shows the spatial context at the maximal deviation of the STA (t = 83 ms prior to spike). Each square is 5° in size. Small insets below show the spatial context before, during and after the context in the large panel.

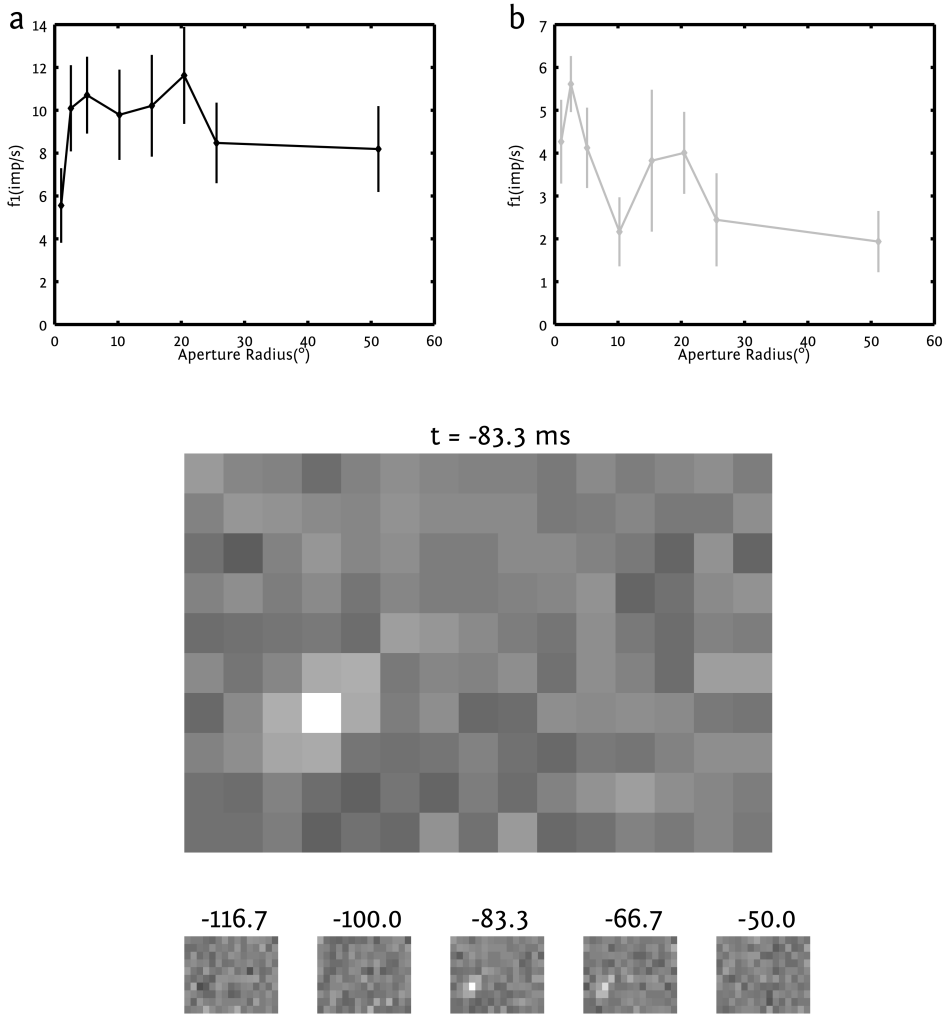

Figure 4.14: **Size Tuning for Neuron ID:42**
The Figure shows size Tuning for Neuron #42. **a** X-Axis is the aperture size in degrees while y-axis is amplitude of the modulation in impulses/s. The nominal contrast used was 1 (in **a**) and 0.25 (in **b**). Also included is the spatio-temporal receptive field (bottom). Large panel shows the spatial context at the maximal deviation of the STA (t = 83 ms prior to spike). Each square is 5° in size. Small insets below show the spatial context before, during and after the context in the large panel.

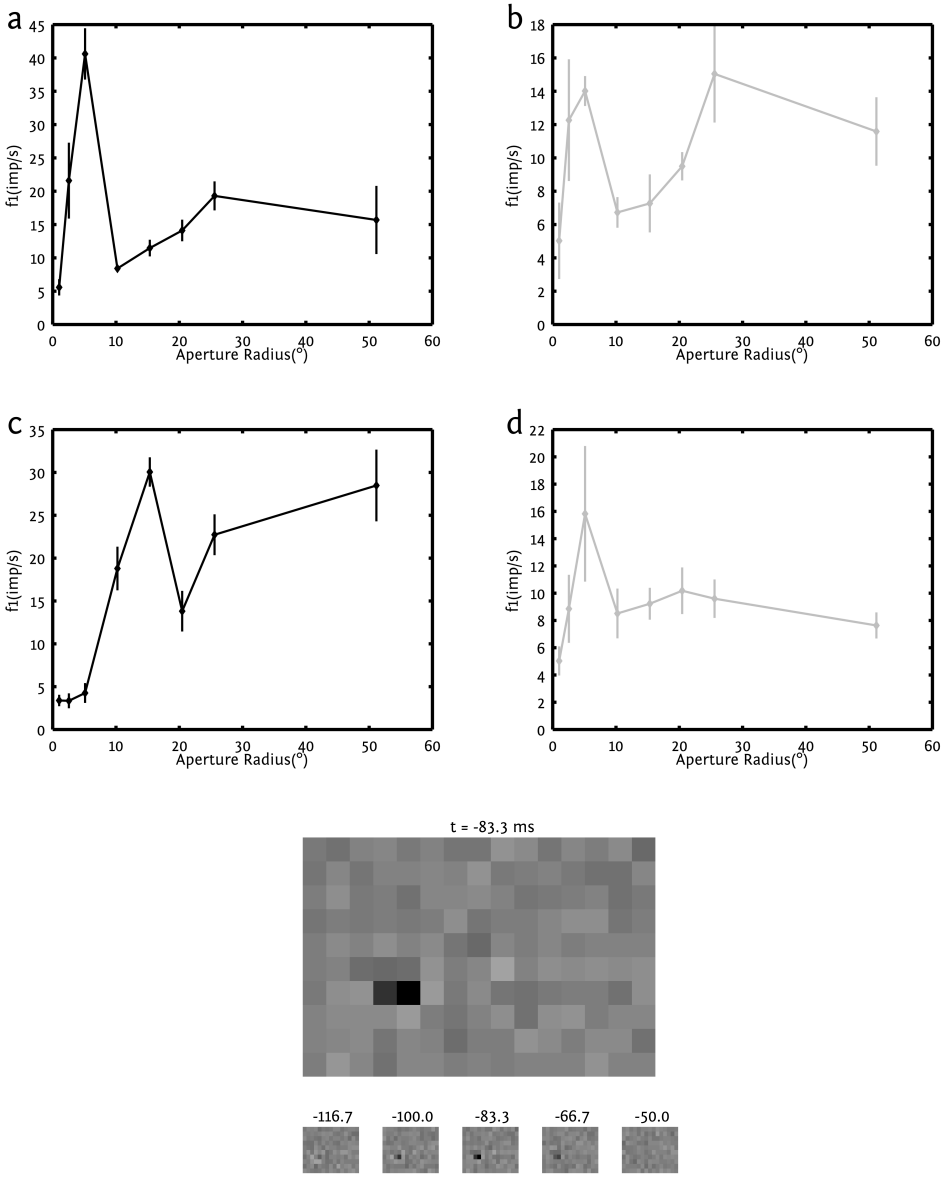

Figure 4.15: **Size Tuning for Neuron ID:43**
The Figure shows size Tuning for Neuron #43. X-Axis is the aperture size in degrees while y-axis is amplitude of the modulation in impulses/s. The nominal contrast used was 1 (in **a** and **c**) and 0.25 (in **b** and **d**). Also included is the spatio-temporal receptive field (bottom). Large panel shows the spatial context at the maximal deviation of the STA (t = 83 ms prior to spike). Each square is 5° in size. Small insets below show the spatial context before, during and after the context in the large panel.

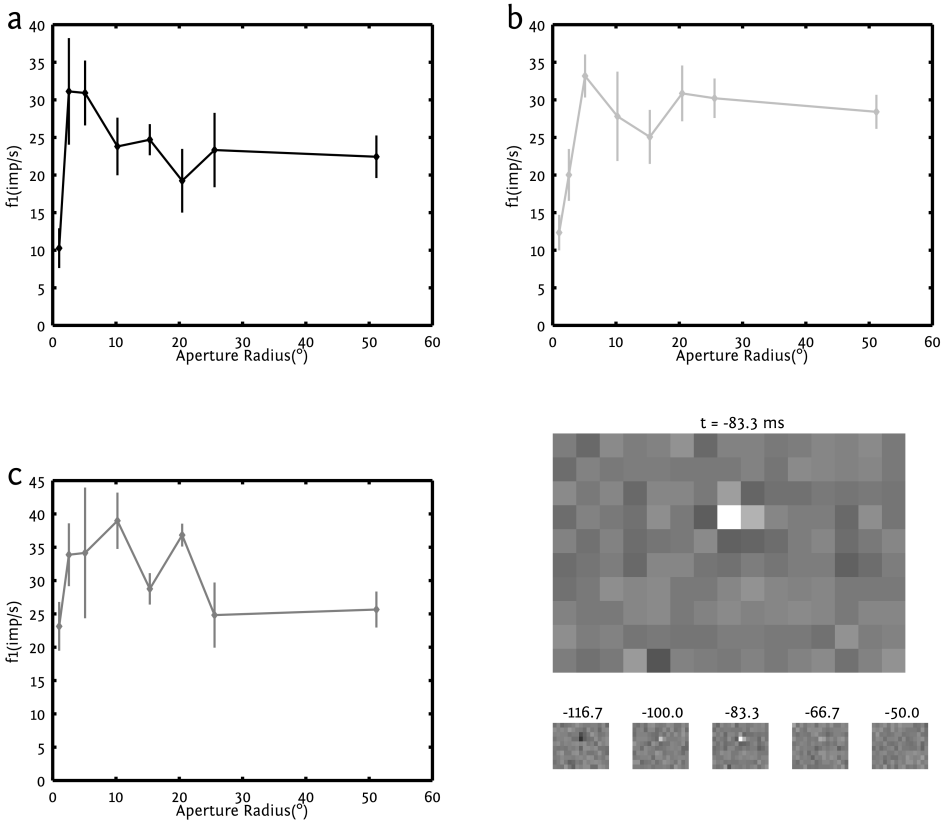

Figure 4.16: **Size Tuning for Neuron ID:45**
The Figure shows size Tuning for Neuron #45. X-Axis is the aperture size in degrees while y-axis is amplitude of the modulation in impulses/s. The nominal contrast used was 1 (in **a**) 0.25 (in **b)** and 0.5 (in **c**). Also included is the spatio-temporal receptive field (bottom right). Large panel shows the spatial context at the maximal deviation of the STA (t = 83 ms prior to spike). Each square is 5° in size. Small insets below show the spatial context before, during and after the context in the large panel.

4.4 Conclusion

How well do the linear DOG models explain size tuning in rodent dLGN neurons? To test this, we used the receptive field fits obtained as shown in 2.2.9 and applied it to the model developed in 3.2.1. Fits were typically poor. Ocassionally, however, the model fit the data at large aperture radii (Figure 4.23).

It still remains to be seen whether simultaneously fitting both the spatial frequency and the area summation is capable of providing reasonable fits to the responses obtained. Also, many of the responses obtained do not scale well with contrast (Figures 4.3,4.4,4.5,4.6,4.13,4.16); and many responses show abnormal increase in activity at high aperture sizes (Figures 4.4 *high contrast*, 4.5 *low contrast*, 4.9a, 4.15c, 4.18a, 4.20a). Such responses are not expected by any of the models described in Chapter 3.

Chapter 4, in part, is being prepared for submission for publication of material. Sriram, Balaji; Reinagel, Pamela. The dissertation author was the primary investigator and the first author of the paper.

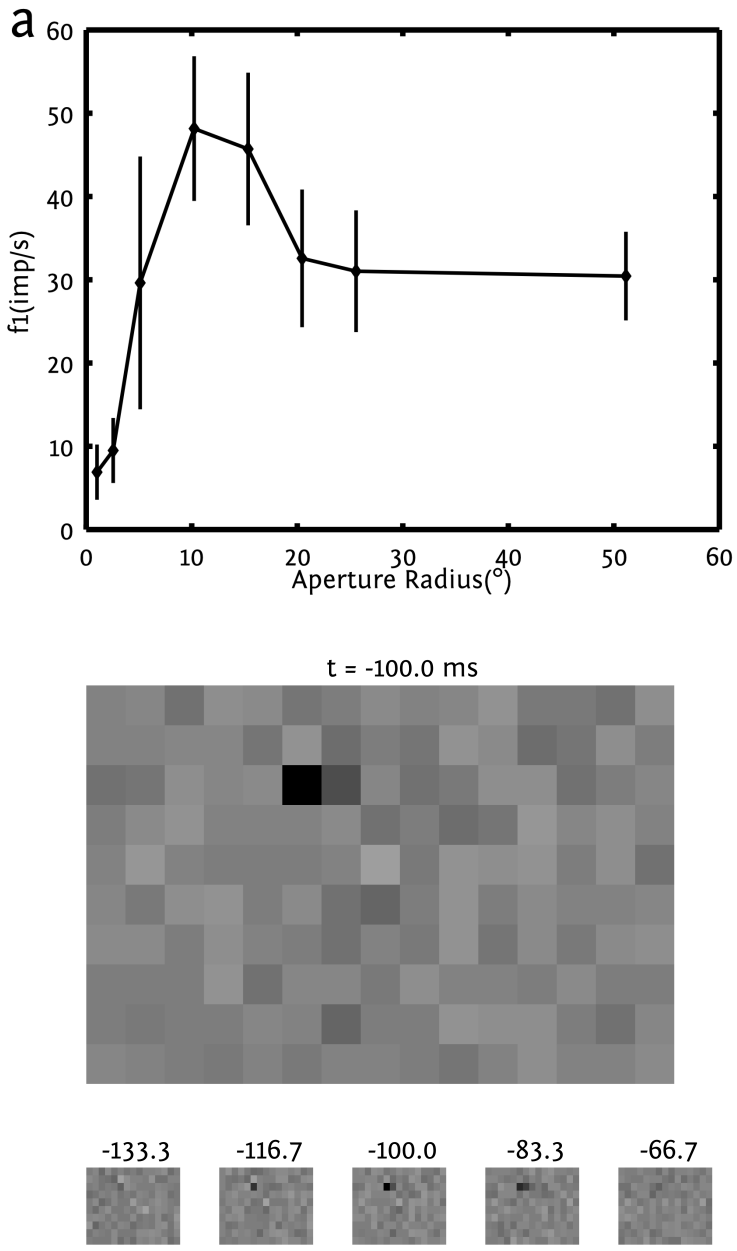

Figure 4.17: **Size Tuning for Neuron ID:46**
The Figure shows size Tuning for Neuron #46. X-Axis is the aperture size in degrees while y-axis is amplitude of the modulation in impulses/s. The nominal contrast used was 1. Also included is the spatio-temporal receptive field (right). Large panel shows the spatial context at the maximal deviation of the STA (t = 100 ms prior to spike). Each square is 5° in size. Small insets below show the spatial context before, during and after the context in the large panel.

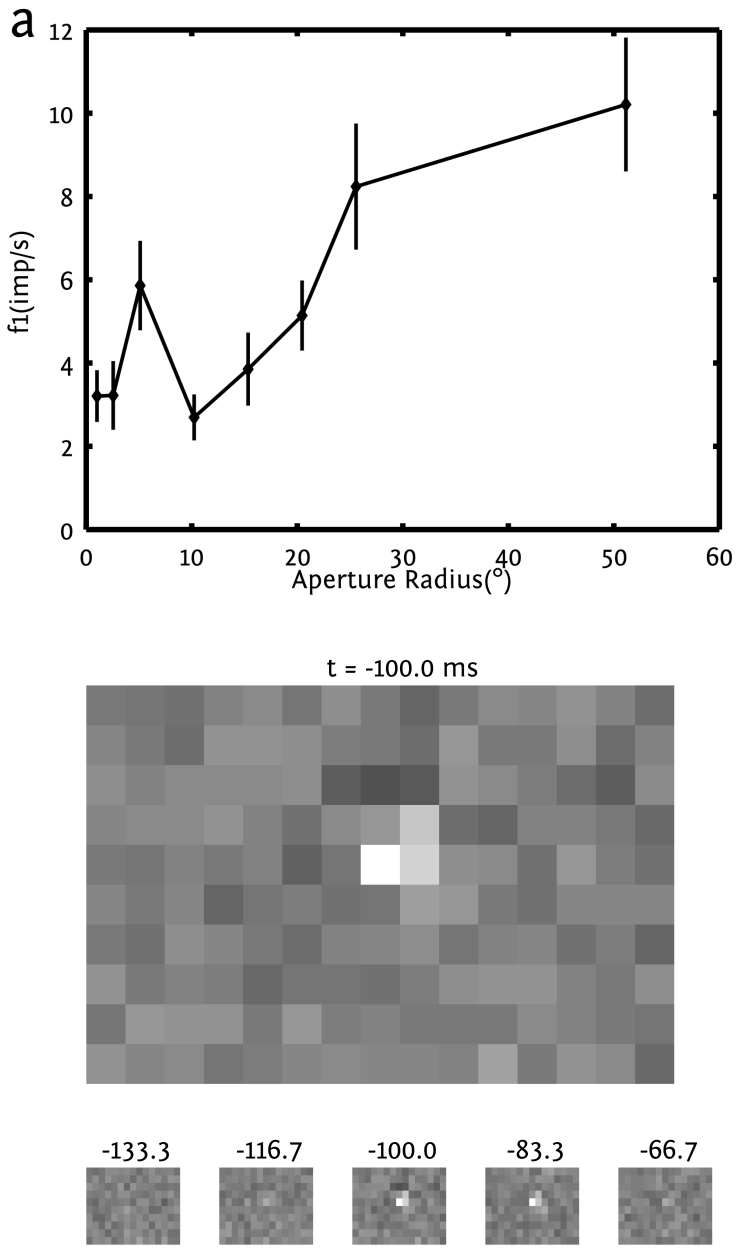

Figure 4.18: **Size Tuning for Neuron ID:48**
The Figure shows size Tuning for Neuron #48. X-Axis is the aperture size in degrees while y-axis is amplitude of the modulation in impulses/s. The nominal contrast used was 1. Also included is the spatio-temporal receptive field (right). Large panel shows the spatial context at the maximal deviation of the STA (t = 100 ms prior to spike). Each square is 5° in size. Small insets below show the spatial context before, during and after the context in the large panel.

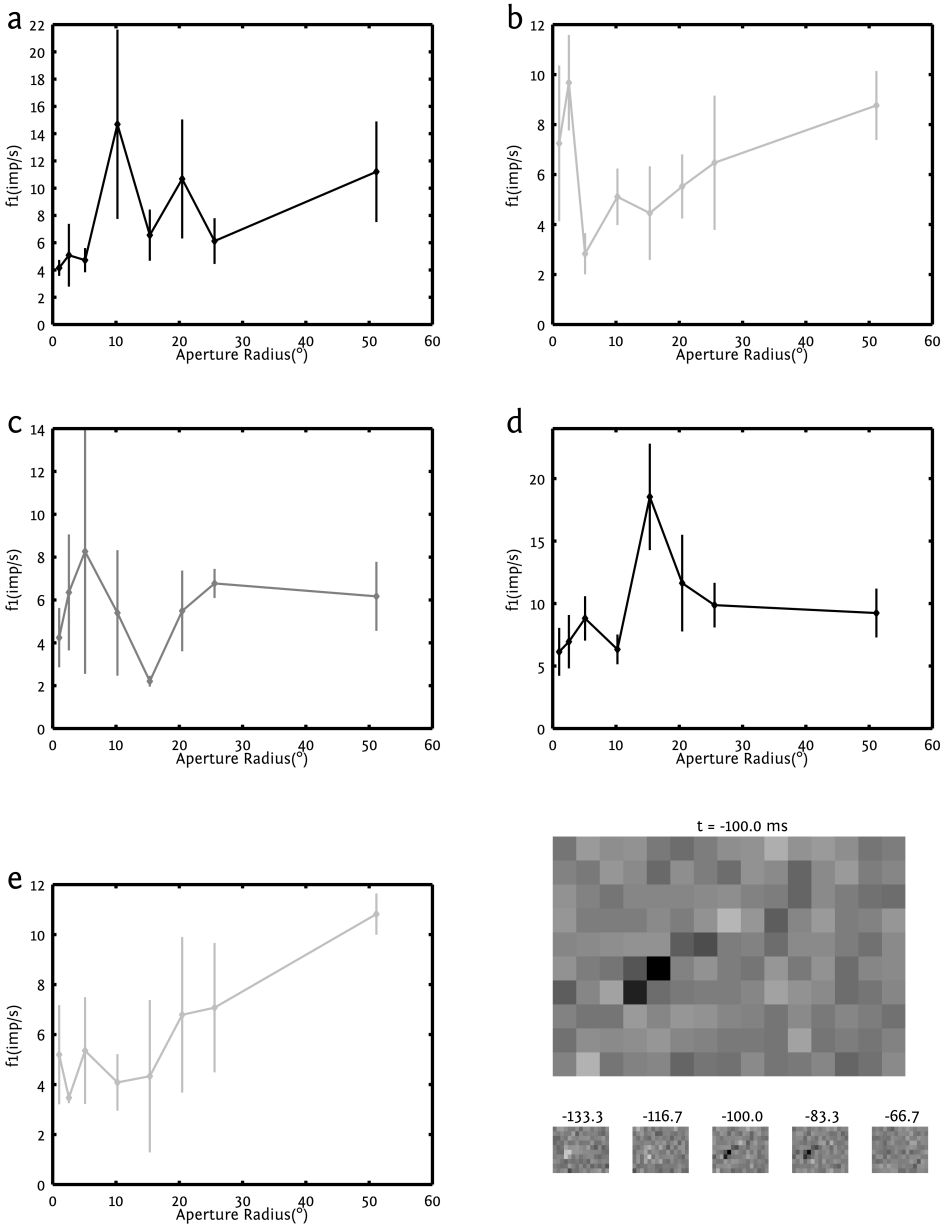

Figure 4.19: **Size Tuning for Neuron ID:58**
The Figure shows size Tuning for Neuron #58. X-Axis is the aperture size in degrees while y-axis is amplitude of the modulation in impulses/s. The nominal contrast used was 1. Also included is the spatio-temporal receptive field (right). Large panel shows the spatial context at the maximal deviation of the STA (t = 100 ms prior to spike). Each square is 5° in size. Small insets below show the spatial context before, during and after the context in the large panel.

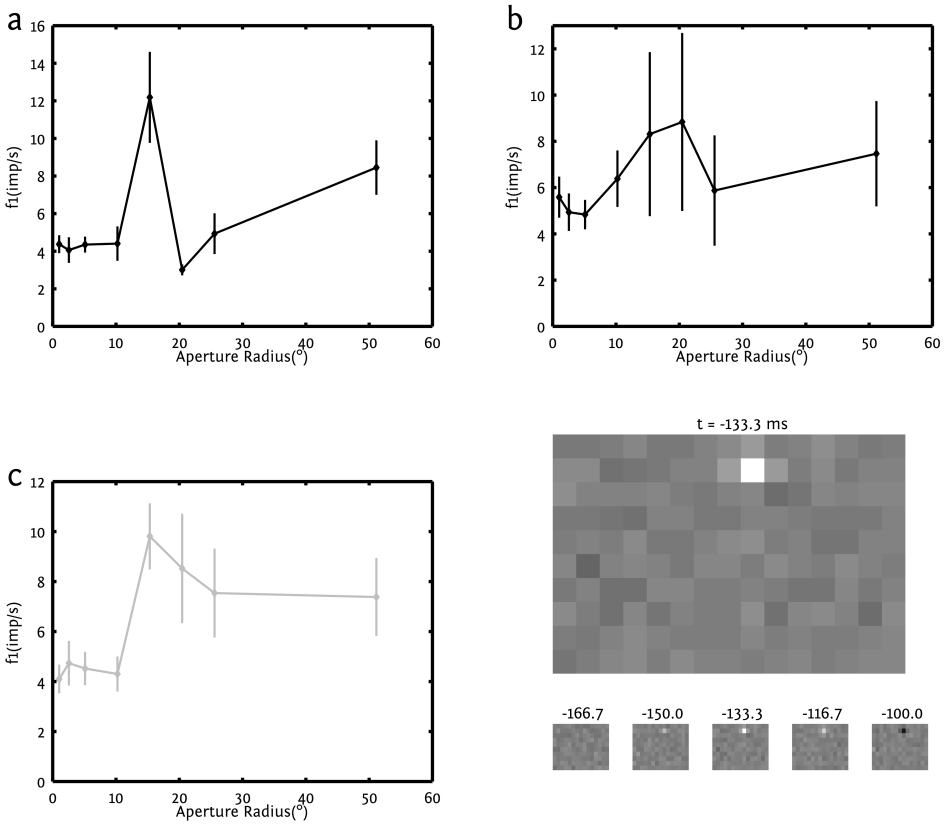

Figure 4.20: **Size Tuning for Neuron ID:63**
The Figure shows size Tuning for Neuron #63. X-Axis is the aperture size in degrees while y-axis is amplitude of the modulation in impulses/s. The nominal contrast used was 1 (in **a** and **b**) and 0.25 (in **c**). Also included is the spatio-temporal receptive field (bottom right). Large panel shows the spatial context at the maximal deviation of the STA (t = 133 ms prior to spike). Each square is 5° in size. Small insets below show the spatial context before, during and after the context in the large panel.

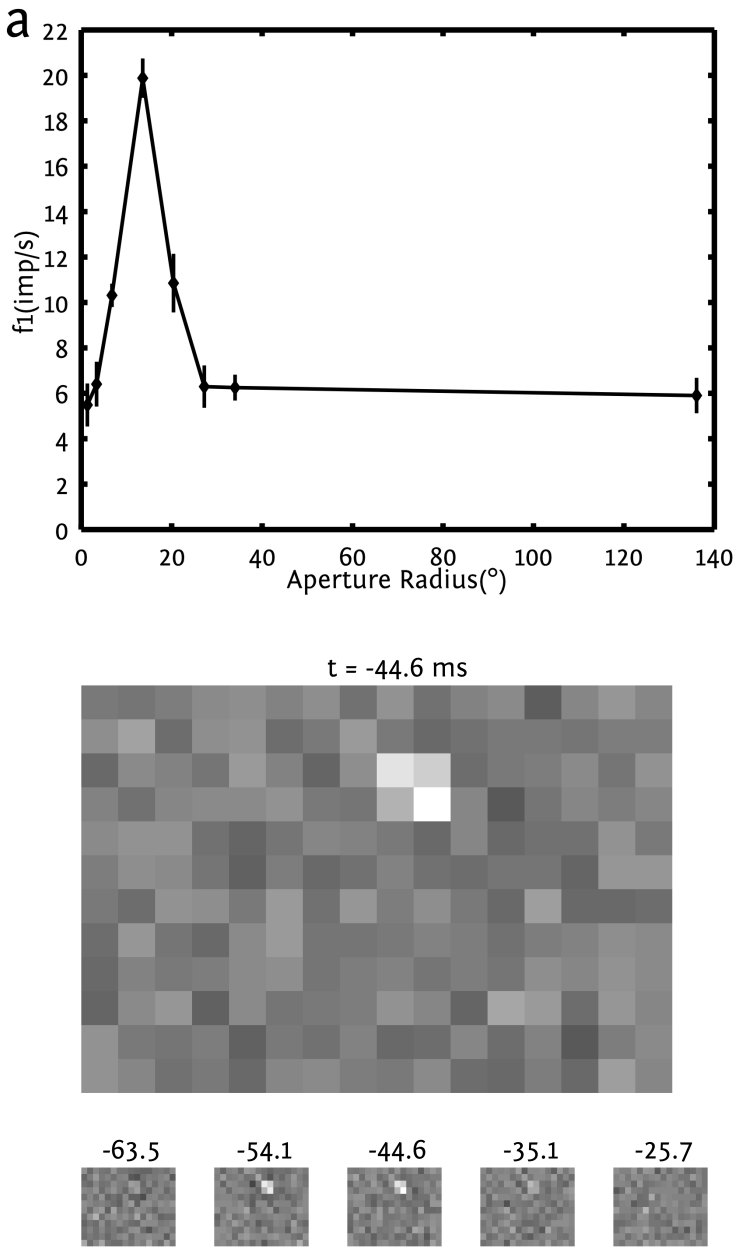

Figure 4.21: **Size Tuning for Neuron ID:75**
The Figure shows size Tuning for Neuron #75. X-Axis is the aperture size in degrees while y-axis is amplitude of the modulation in impulses/s. The nominal contrast used was 1. Also included is the spatio-temporal receptive field (right). Large panel shows the spatial context at the maximal deviation of the STA (t = 100 ms prior to spike). Each square is 2.5° in size. Small insets below show the spatial context before, during and after the context in the large panel.

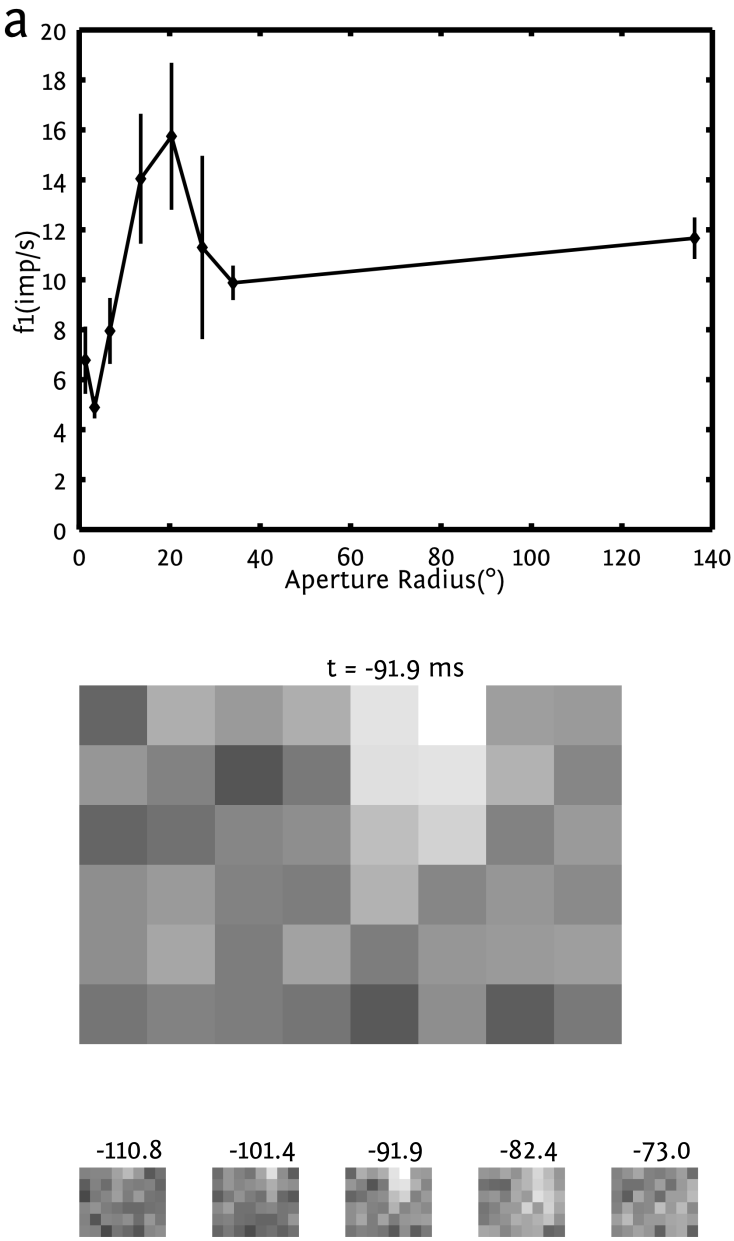

Figure 4.22: **Size Tuning for Neuron ID:76**
The Figure shows size Tuning for Neuron #76. X-Axis is the aperture size in degrees while y-axis is amplitude of the modulation in impulses/s. The nominal contrast used was 1. Also included is the spatio-temporal receptive field (right). Large panel shows the spatial context at the maximal deviation of the STA (t = 100 ms prior to spike). Each square is 5° in size. Small insets below show the spatial context before, during and after the context in the large panel.

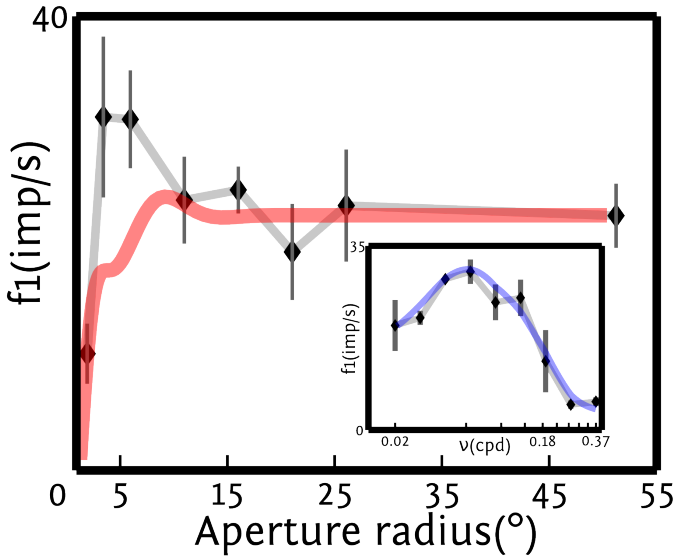

Figure 4.23: **Fit to Size Tuning for Neuron ID:45** The Figure shows fit to size tuning obtained form the model fit to the Spatia frequency tuning curve (inset). Data is shown in black with grey error bars ($mean \pm SEM$) while fit is shown in red.

Bibliography

[Alitto et al., 2011] Alitto, H. J., Moore, B. D. t., Rathbun, D. L., and Usrey, W. M. (2011). A comparison of visual responses in the lateral geniculate nucleus of alert and anaesthetized macaque monkeys. *J Physiol*, 589(Pt 1):87–99.

[Alitto and Usrey, 2003] Alitto, H. J. and Usrey, W. M. (2003). Corticothalamic feedback and sensory processing. *Curr. Opin. Neurobiol.*, 13(4):440–445.

[Alitto and Usrey, 2005] Alitto, H. J. and Usrey, W. M. (2005). Dynamic properties of thalamic neurons for vision. *Prog. Brain Res.*, 149:83–90.

[Anderson and Yoshida, 1977] Anderson, M. and Yoshida, M. (1977). Electrophysiological evidence for branching nigral projections to the thalamus and the superior colliculus. *Brain Res*, 137(2):361–4.

[Andolina et al., 2007] Andolina, I. M., Jones, H. E., Wang, W., and Sillito, A. M. (2007). Corticothalamic feedback enhances stimulus response precision in the visual system. *Proc. Natl. Acad. Sci. U.S.A.*, 104(5):1685–1690.

[Atick, 2011] Atick, J. J. (2011). Could information theory provide an ecological theory of sensory processing? *Network*, 22(1-4):4–44.

[Atick and Redlich, 1992] Atick, J. J. and Redlich, A. N. (1992). What does the retina know about natural scenes? *Neural Computation*, 4(2):196–210.

[Attneave, 1954] Attneave, F. (1954). Some informational aspects of visual perception. *Psychol Rev*, 61(3):183–93.

[Barlow, 1961] Barlow, H. (1961). Possible principles underlying the transformations of sensory messages. *Sensory Communication*, 1:217–234.

[Barlow, 2001] Barlow, H. (2001). Redundancy reduction revisited. *Network*, 12(3):241–253.

[Bellavance et al., 2010] Bellavance, M.-A., Demers, M., and Deschênes, M. (2010). Feedforward inhibition determines the angular tuning of vibrissal responses in the principal trigeminal nucleus. *J Neurosci*, 30(3):1057–63.

[Bonin et al., 2005] Bonin, V., Mante, V., and Carandini, M. (2005). The suppressive field of neurons in lateral geniculate nucleus. *J. Neurosci.*, 25(47):10844–10856.

[Brainard, 1997] Brainard, D. H. (1997). The psychophysics toolbox. *Spat Vis*, 10(4):433–6.

[Busse et al., 2011] Busse, L., Ayaz, A., Dhruv, N. T., Katzner, S., Saleem, A. B., Schölvinck, M. L., Zaharia, A. D., and Carandini, M. (2011). The detection of visual contrast in the behaving mouse. *J Neurosci*, 31(31):11351–61.

[Butts et al., 2011] Butts, D. A., Weng, C., Jin, J., Alonso, J. M., and Paninski, L. (2011). Temporal precision in the visual pathway through the interplay of excitation and stimulus-driven suppression. *J. Neurosci.*, 31(31):11313–11327.

[Cai et al., 1997] Cai, D., DeAngelis, G. C., and Freeman, R. D. (1997). Spatiotemporal receptive field organization in the lateral geniculate nucleus of cats and kittens. *J. Neurophysiol.*, 78(2):1045–1061.

[Carandini et al., 1997] Carandini, M., Heeger, D. J., and Movshon, J. A. (1997). Linearity and normalization in simple cells of the macaque primary visual cortex. *J. Neurosci.*, 17(21):8621–8644.

[Cavanaugh et al., 2002a] Cavanaugh, J. R., Bair, W., and Movshon, J. A. (2002a). Nature and interaction of signals from the receptive field center and surround in macaque V1 neurons. *J. Neurophysiol.*, 88(5):2530–2546.

[Cavanaugh et al., 2002b] Cavanaugh, J. R., Bair, W., and Movshon, J. A. (2002b). Selectivity and spatial distribution of signals from the receptive field surround in macaque V1 neurons. *J. Neurophysiol.*, 88(5):2547–2556.

[Chelazzi et al., 1989] Chelazzi, L., Rossi, F., Tempia, F., Ghirardi, M., and Strata, P. (1989). Saccadic Eye Movements and Gaze Holding in the Head-Restrained Pigmented Rat. *Eur. J. Neurosci.*, 1(6):639–646.

[Cheng et al., 1995] Cheng, H., Chino, Y. M., Smith, E. L. r., Hamamoto, J., and Yoshida, K. (1995). Transfer characteristics of lateral geniculate nucleus x neurons in the cat: effects of spatial frequency and contrast. *J Neurophysiol*, 74(6):2548–57.

[Chichilnisky, 2001] Chichilnisky, E. J. (2001). A simple white noise analysis of neuronal light responses. *Network*, 12(2):199–213.

[Cornelissen et al., 2002] Cornelissen, F. W., Peters, E. M., and Palmer, J. (2002). The Eyelink Toolbox: eye tracking with MATLAB and the Psychophysics Toolbox. *Behav Res Methods Instrum Comput*, 34(4):613–617.

[Creer et al., 2010] Creer, D. J., Romberg, C., Saksida, L. M., van Praag, H., and Bussey, T. J. (2010). Running enhances spatial pattern separation in mice. *Proc Natl Acad Sci U S A*, 107(5):2367–72.

[Croner and Kaplan, 1995] Croner, L. J. and Kaplan, E. (1995). Receptive fields of P and M ganglion cells across the primate retina. *Vision Res.*, 35(1):7–24.

[Dacey et al., 2000] Dacey, D., Packer, O. S., Diller, L., Brainard, D., Peterson, B., and Lee, B. (2000). Center surround receptive field structure of cone bipolar cells in primate retina. *Vision Res*, 40(14):1801–11.

[Dan et al., 1996] Dan, Y., Atick, J. J., and Reid, R. C. (1996). Efficient coding of natural scenes in the lateral geniculate nucleus: experimental test of a computational theory. *J Neurosci*, 16(10):3351–62.

[Dawis et al., 1984] Dawis, S., Shapley, R., Kaplan, E., and Tranchina, D. (1984). The receptive field organization of X-cells in the cat: spatiotemporal coupling and asymmetry. *Vision Res.*, 24(6):549–564.

[DiCarlo et al., 1998] DiCarlo, J. J., Johnson, K. O., and Hsiao, S. S. (1998). Structure of receptive fields in area 3b of primary somatosensory cortex in the alert monkey. *J Neurosci*, 18(7):2626–45.

["Discenza, 2011] "Discenza, C. (2011). *Substructure within the dorsal lateral geniculate nucleus of the pigmented rat*. PhD thesis, University of California, San Diego.

[Enroth-Cugell and Robson, 1966] Enroth-Cugell, C. and Robson, J. G. (1966). The contrast sensitivity of retinal ganglion cells of the cat. *J. Physiol. (Lond.)*, 187(3):517–552.

[Flister and Reinagel, 2010] Flister, E. and Reinagel, P. (2010). Bursts and visual encoding in lgn during natural state fluctuations in the unanesthetized rat. In *Computational and Systems Neuroscience 2010. Salt Lake City, Utah.*

[Freeman et al., 2002] Freeman, T. C., Durand, S., Kiper, D. C., and Carandini, M. (2002). Suppression without inhibition in visual cortex. *Neuron*, 35(4):759–771.

[Fukuda et al., 1979] Fukuda, Y., Sumitomo, I., Sugitani, M., and Iwama, K. (1979). Receptive-field properties of cells in the dorsal part of the albino rat's lateral geniculate nucleus. *Jpn J Physiol*, 29(3):283–307.

[Graham et al., 2006] Graham, D. J., Chandler, D. M., and Field, D. J. (2006). Can the theory of "whitening" explain the center-surround properties of retinal ganglion cell receptive fields? *Vision Res.*, 46(18):2901–2913.

[Grubb and Thompson, 2003] Grubb, M. S. and Thompson, I. D. (2003). Quantitative characterization of visual response properties in the mouse dorsal lateral geniculate nucleus. *J Neurophysiol*, 90(6):3594–607.

[Harris et al., 2000] Harris, K. D., Henze, D. A., Csicsvari, J., Hirase, H., and Buzsaki, G. (2000). Accuracy of tetrode spike separation as determined by simultaneous intracellular and extracellular measurements. *J. Neurophysiol.*, 84(1):401–414.

[Hartline et al., 1956] Hartline, H. K., Wagner, H. G., and Ratliff, F. (1956). Inhibition in the eye of limulus. *J Gen Physiol*, 39(5):651–73.

[Harvey, 2012] Harvey, S. J. (2012). Models for studies of proteoglycans in kidney pathophysiology. *Methods Mol Biol*, 836:259–84.

[Heeger, 1992] Heeger, D. J. (1992). Normalization of cell responses in cat striate cortex. *Vis. Neurosci.*, 9(2):181–197.

[Heine and Passaglia, 2011] Heine, W. F. and Passaglia, C. L. (2011). Spatial receptive field properties of rat retinal ganglion cells. *Vis Neurosci*, 28(5):403–17.

[Hikosaka and Sakamoto, 1987] Hikosaka, O. and Sakamoto, M. (1987). Dynamic characteristics of saccadic eye movements in the albino rat. *Neurosci. Res.*, 4(4):304–308.

[Hubel and Wiesel, 1961] Hubel, D. H. and Wiesel, T. N. (1961). Integrative action in the cat's lateral geniculate body. *J Physiol*, 155:385–98.

[Jones et al., 2000] Jones, H. E., Andolina, I. M., Oakely, N. M., Murphy, P. C., and Sillito, A. M. (2000). Spatial summation in lateral geniculate nucleus and visual cortex. *Exp Brain Res*, 135(2):279–284.

[Jones and Sillito, 1991] Jones, H. E. and Sillito, A. M. (1991). The length-response properties of cells in the feline dorsal lateral geniculate nucleus. *J. Physiol. (Lond.)*, 444:329–348.

[Karklin and Simoncelli, 2011] Karklin, Y. and Simoncelli, E. (2011). Efficient coding of natural images with a population of noisy linear-nonlinear neurons. In *Adv in Neural Information Processing Systems (NIPS), 2011*.

[Keat et al., 2001] Keat, J., Reinagel, P., Reid, R. C., and Meister, M. (2001). Predicting every spike: a model for the responses of visual neurons. *Neuron*, 30(3):803–817.

[Kleiner et al., 2007] Kleiner, M., Brainard, D., and Pelli, D. (2007). What's new in psychtoolbox-3? In *European Conference of Visual Perception*.

[Knudsen and Konishi, 1978] Knudsen, E. I. and Konishi, M. (1978). Center-surround organization of auditory receptive fields in the owl. *Science*, 202(4369):778–80.

[Kriebel, 1975] Kriebel, R. M. (1975). Neurons of the dorsal lateral geniculate nucleus of the albino rat. *J Comp Neurol*, 159(1):45–67.

[Kuang et al., 2012] Kuang, X., Poletti, M., Victor, J. D., and Rucci, M. (2012). Temporal encoding of spatial information during active visual fixation. *Curr Biol*, 22(6):510–4.

[Kuffler, 1953] Kuffler, S. W. (1953). Discharge patterns and functional organization of mammalian retina. *J Neurophysiol*, 16(1):37–68.

[Lennie and Perry, 1981] Lennie, P. and Perry, V. H. (1981). Spatial contrast sensitivity of cells in the lateral geniculate nucleus of the rat. *J Physiol*, 315:69–79.

[LeVay and Ferster, 1979] LeVay, S. and Ferster, D. (1979). Proportion of interneurons in the cat's lateral geniculate nucleus. *Brain Res.*, 164:304–308.

[Levick et al., 1972] Levick, W. R., Cleland, B. G., and Dubin, M. W. (1972). Lateral geniculate neurons of cat: retinal inputs and physiology. *Invest Ophthalmol*, 11(5):302–311.

[Lindstrom and Wrobel, 2011] Lindstrom, S. and Wrobel, A. (2011). Feedforward and recurrent inhibitory receptive fields of principal cells in the cat's dorsal lateral geniculate nucleus. *Pflugers Arch.*, 461(2):277–294.

[Linsenmeier et al., 1982] Linsenmeier, R. A., Frishman, L. J., Jakiela, H. G., and Enroth-Cugell, C. (1982). Receptive field properties of x and y cells in the cat retina derived from contrast sensitivity measurements. *Vision Res.*, 22(9):1173–1183.

[Livingstone and Hubel, 1981] Livingstone, M. S. and Hubel, D. H. (1981). Effects of sleep and arousal on the processing of visual information in the cat. *Nature*, 291(5816):554–561.

[Maffei and Fiorentini, 1973] Maffei, L. and Fiorentini, A. (1973). The visual cortex as a spatial frequency analyser. *Vision Res.*, 13(7):1255–1267.

[McAlonan et al., 2008] McAlonan, K., Cavanaugh, J., and Wurtz, R. H. (2008). Guarding the gateway to cortex with attention in visual thalamus. *Nature*, 456(7220):391–394.

[Meier et al., 2011] Meier, P., Flister, E., and Reinagel, P. (2011). Collinear features impair visual detection by rats. *J Vis*, 11(3).

[Morozov, 2008] Morozov, A. (2008). Conditional gene expression and targeting in neuroscience research. *Curr Protoc Neurosci*, Chapter 4:Unit 4.31.

[Morrone et al., 1982] Morrone, M. C., Burr, D. C., and Maffei, L. (1982). Functional implications of cross-orientation inhibition of cortical visual cells. I. Neurophysiological evidence. *Proc. R. Soc. Lond., B, Biol. Sci.*, 216(1204):335–354.

[Muller and Dacheux, 1997] Muller, J. F. and Dacheux, R. F. (1997). Alpha ganglion cells of the rabbit retina lose antagonistic surround responses under dark adaptation. *Vis. Neurosci.*, 14(2):395–401.

[Murphy and Sillito, 1987] Murphy, P. C. and Sillito, A. M. (1987). Corticofugal feedback influences the generation of length tuning in the visual pathway. *Nature*, 329(6141):727–729.

[Nolt et al., 2004] Nolt, M. J., Kumbhani, R. D., and Palmer, L. A. (2004). Contrast-dependent spatial summation in the lateral geniculate nucleus and retina of the cat. *J. Neurophysiol.*, 92(3):1708–1717.

[O'Keefe et al., 1998] O'Keefe, L. P., Levitt, J. B., Kiper, D. C., Shapley, R. M., and Movshon, J. A. (1998). Functional organization of owl monkey lateral geniculate nucleus and visual cortex. *J. Neurophysiol.*, 80(2):594–609.

[Olsen et al., 2012] Olsen, S. R., Bortone, D. S., Adesnik, H., and Scanziani, M. (2012). Gain control by layer six in cortical circuits of vision. *Nature*, 483(7387):47–52.

[Olshausen and Field, 1996a] Olshausen, B. A. and Field, D. J. (1996a). Emergence of simple-cell receptive field properties by learning a sparse code for natural images. *Nature*, 381(6583):607–9.

[Olshausen and Field, 1996b] Olshausen, B. A. and Field, D. J. (1996b). Natural image statistics and efficient coding. *Network*, 7(2):333–9.

[Pape and Eysel, 1988] Pape, H. C. and Eysel, U. T. (1988). Cholinergic excitation and inhibition in the visual thalamus of the cat–influences of cortical inactivation and barbiturate anesthesia. *Brain Res.*, 440(1):79–86.

["Paxinos and Watson, 2006] "Paxinos, G. and Watson, C. (2006). *The Rat Brain in Stereotaxic Coordinates - The New Coronal Set, Fifth Edition*. Elsevier.

[Pelli, 1997] Pelli, D. G. (1997). The videotoolbox software for visual psychophysics: transforming numbers into movies. *Spat Vis*, 10(4):437–42.

[Pitkow and Meister, 2012] Pitkow, X. and Meister, M. (2012). Decorrelation and efficient coding by retinal ganglion cells. *Nat Neurosci*, 15(4):628–35.

[Puchalla et al., 2005] Puchalla, J. L., Schneidman, E., Harris, R. A., and Berry, M. J. (2005). Redundancy in the population code of the retina. *Neuron*, 46(3):493–504.

[Reinagel and Zador, 1999] Reinagel, P. and Zador, A. M. (1999). Natural scene statistics at the centre of gaze. *Network*, 10(4):341–350.

[Rodieck, 1965] Rodieck, R. W. (1965). Quantitative analysis of cat retinal ganglion cell response to visual stimuli. *Vision Res.*, 5(11):583–601.

[Rodieck and Stone, 1965] Rodieck, R. W. and Stone, J. (1965). Analysis of receptive fields of cat retinal ganglion cells. *J. Neurophysiol.*, 28(5):832–849.

[Sceniak et al., 2006] Sceniak, M. P., Chatterjee, S., and Callaway, E. M. (2006). Visual spatial summation in macaque geniculocortical afferents. *J. Neurophysiol.*, 96(6):3474–3484.

[Sceniak et al., 2001] Sceniak, M. P., Hawken, M. J., and Shapley, R. (2001). Visual spatial characterization of macaque V1 neurons. *J. Neurophysiol.*, 85(5):1873–1887.

[Sclar et al., 1990] Sclar, G., Maunsell, J. H., and Lennie, P. (1990). Coding of image contrast in central visual pathways of the macaque monkey. *Vision Res.*, 30(1):1–10.

[Sekirnjak et al., 2011] Sekirnjak, C., Jepson, L. H., Hottowy, P., Sher, A., Dabrowski, W., Litke, A. M., and Chichilnisky, E. J. (2011). Changes in physiological properties of rat ganglion cells during retinal degeneration. *J. Neurophysiol.*, 105(5):2560–2571.

[Sillito et al., 2006] Sillito, A. M., Cudeiro, J., and Jones, H. E. (2006). Always returning: feedback and sensory processing in visual cortex and thalamus. *Trends Neurosci.*, 29(6):307–316.

[Sillito et al., 1993] Sillito, A. M., Cudeiro, J., and Murphy, P. C. (1993). Orientation sensitive elements in the corticofugal influence on centre-surround interactions in the dorsal lateral geniculate nucleus. *Exp Brain Res*, 93(1):6–16.

[Sillito et al., 1995] Sillito, A. M., Grieve, K. L., Jones, H. E., Cudeiro, J., and Davis, J. (1995). Visual cortical mechanisms detecting focal orientation discontinuities. *Nature*, 378(6556):492–496.

[Simons and Carvell, 1989] Simons, D. J. and Carvell, G. E. (1989). Thalamocortical response transformation in the rat vibrissa/barrel system. *J Neurophysiol*, 61(2):311–30.

[Solomon et al., 2002] Solomon, S. G., White, A. J., and Martin, P. R. (2002). Extraclassical receptive field properties of parvocellular, magnocellular, and koniocellular cells in the primate lateral geniculate nucleus. *J. Neurosci.*, 22(1):338–349.

[Soo et al., 2011] Soo, F. S., Schwartz, G. W., Sadeghi, K., and Berry, M. J. (2011). Fine spatial information represented in a population of retinal ganglion cells. *J. Neurosci.*, 31(6):2145–2155.

[Sriram et al., 2011] Sriram, B., Meier, P., and Reinagel, P. (2011). Visual response properties of neurons in the rat lgn. In *Computational and Systems Neuroscience 2011. Salt Lake City, Utah.*

[Thomas and Capecchi, 1987] Thomas, K. R. and Capecchi, M. R. (1987). Site-directed mutagenesis by gene targeting in mouse embryo-derived stem cells. *Cell*, 51(3):503–12.

[van Hateren, 1992] van Hateren, J. H. (1992). A theory of maximizing sensory information. *Biol Cybern*, 68(1):23–9.

[Victor, 1987] Victor, J. D. (1987). The dynamics of the cat retinal X cell centre. *J. Physiol. (Lond.)*, 386:219–246.

[Wang et al., 2007] Wang, X., Wei, Y., Vaingankar, V., Wang, Q., Koepsell, K., Sommer, F. T., and Hirsch, J. A. (2007). Feedforward excitation and inhibition evoke dual modes of firing in the cat's visual thalamus during naturalistic viewing. *Neuron*, 55(3):465–478.

[Wilson et al., 1996] Wilson, J. R., Forestner, D. M., and Cramer, R. P. (1996). Quantitative analyses of synaptic contacts of interneurons in the dorsal lateral geniculate nucleus of the squirrel monkey. *Vis. Neurosci.*, 13(6):1129–1142.

[Xu et al., 2002] Xu, X., Bonds, A. B., and Casagrande, V. A. (2002). Modeling receptive-field structure of koniocellular, magnocellular, and parvocellular LGN cells in the owl monkey (Aotus trivigatus). *Vis. Neurosci.*, 19(6):703–711.

[Zoccolan et al., 2009] Zoccolan, D., Oertelt, N., DiCarlo, J. J., and Cox, D. D. (2009). A rodent model for the study of invariant visual object recognition. *Proc Natl Acad Sci U S A*, 106(21):8748–53.